Beyond 5G White Paper
6G Radio Technology Project
“Terminal-Cooperative MIMO Technology”

Version 1.1

September 30, 2025

XG Mobile Promotion Forum

Preface **6**

I. Research Trends in Terminal Collaborative Technology **9**

I-1. Significance of Applying Terminal Collaborative Technology 9

I-2. Standard Models of Terminal Collaborative Technology 9

I-2.1. Downlink Terminal Collaborative MIMO Signal Reception 9

I-2.2. Uplink Terminal Collaborative MIMO Signal Transmission 10

I-2.3. Uplink Terminal Collaborative Beamforming Signal Transmission 11

I-3. Technical Issues in Terminal Collaborative Technology 11

I-3.1. Common Technical Issues 11

I-3.2. Technical Issues in Downlink Terminal Collaborative MIMO Signal Reception 13

I-3.3. Technical Issues in Uplink Terminal Collaborative MIMO Signal Transmission 13

I-3.4. Technical Issues in Uplink Terminal Collaborative Beamforming Signal Transmission. 13

REFERENCES 14

II. Recent Advances in Terminal Collaborative Technology in Japan **16**

II-1. Terminal Collaborative Transmission Project 17

II-1.1. Terminal-Collaborated MIMO Reception 18

II-1.1.1. Introduction 18

II-1.1.2. System Model 19

II-1.1.3. Subband-based signal processing and performance 20

II-1.1.4. Conclusion 23

REFERENCE 23

II-1.2. Filter-and-Forward Collaborative Relaying For Higher Spectrum Efficiency 25

II-1.2.1. Introduction 25

II-1.2.2. Configuration of Proposed Filter-and-Forward Collaborative Relaying 26

II-1.2.3. Signal to Noise Power Ratio Estimation at Destination Terminal 26
II-1.2.4. Relay Section 27
II-1.2.5. Computer Simulation.....27
II-1.2.6. Conclusion.....29
REFERENCE.....29
II-1.3. Wireless Security for Terminal Collaborative Communication System 31
II-1.3.1. Introduction 31
II-1.3.2. Terminal Cooperative Communication System Applying Chaos Modulation Scheme.....32
II-1.3.3. Numerical results.....34
II-1.3.4. Summary.....37
REFERENCE.....37
II-1.4. Phase Noise Compensation with Time Window Averaging for CTFI-OFDM 39
II-1.4.1. Introduction 39
II-1.4.2. System Model 40
II-1.4.3. Phase Noise Compensation with Time Window Averaging 41
II-1.4.4. Computer Simulation Results 42
II-1.4.5. Conclusion.....43
REFERENCE.....43
II-1.5. Cooperative Positioning with User-Terminal Collaboration 45
II-1.5.1. Introduction 45
II-1.5.2. System Model and Technical Details.....46
II-1.5.3. Localization Methodology 47
II-1.5.4. Performance Evaluation 48
II-1.5.5. Conclusion.....50
REFERENCES 50
II-1.6. Access Control for Terminal Collaborative Communication System 52
II-1.6.1. Introduction 52
II-1.6.2. System Model 53

II-1.6.3. Access Control 54
II-1.6.4. Numerical Results 54
II-1.6.5. Conclusion 55
REFERENCE 56
II-1.7. Terminal Grouping Based on Instantaneous Throughput 57
II-1.7.1. Introduction 57
II-1.7.2. System Model 57
II-1.7.3. Grouping Scheme 58
II-1.7.4. Performance Evaluation 59
II-1.7.5. Conclusions 61
REFERENCE 61
II-1.8. Impact of Signaling Overhead in Uplink Collaborative MIMO Transmission 62
II-1.8.1. Introduction 62
II-1.8.2. System Model 63
II-1.8.3. Procedure for Collaborative MIMO Uplink Transmission 63
II-1.8.4. Performance Evaluation 66
II-1.8.5. Conclusion 69
REFERENCE 69
II-2. Virtualized Terminal Technology using Terahertz-Band for Ultra High Capacity towards Beyond 5G and 6G 70
II-2.1. Introduction 70
II-2.2. Virtualized Terminal using THz-band 71
II-2.3. Simulation Evaluation 73
II-2.4. Experimental Results 75
II-2.5. Conclusion 77
Acknowledgement 78
REFERENCE 78
II-3. Performance of Collaborative MIMO Reception: Initial Results of 25.9GHz Collaboration 79
II-3.1. Introduction 79

II-3.2. System Model 80
II-3.3. Measurement Campaign 80
II-3.4. Experimental Results 83
II-3.5. Conclusion 83
Acknowledgements 83
REFERENCE 83
Abbreviation List 86

【Revision History】

Ver.	Date	Contents	Note
1.0	2025.5.28	Initial version	
1.1	2025.9.30	Revised version	

Preface

Terminal-cooperative MIMO technology, which in this context refers to a system where user terminals/devices jointly collaborate/cooperate[1] to improve MIMO transmission performance, is a relatively new concept. This study addresses the challenge of limited frequency bands suitable for mobile communication—those with favorable radio propagation characteristics—by integrating multiple key advancements: the capacity-scaling properties of multiple-input multiple-output (MIMO) transmission, the proliferation of advanced digital radios in high-demand areas, and the emergence of high-frequency, low-latency, short-range communication technologies.

Traditionally, high-performance digital radios independently communicate with base stations, thereby competing for shared wireless resources. However, with recent advancements enabling these terminals to support high-speed, low-latency communication over short distances, it is now feasible for nearby devices to collaborate and form a collaborative system. In this configuration, the devices act as a unified, high-capacity virtual terminal with a large number of antennas. This collaborative framework significantly enhances the communication capacity with the base station through MIMO techniques.

Notably, this approach allows for the efficient utilization of valuable frequency bands characterized by excellent propagation properties but relatively long wavelengths-bands that have traditionally posed challenges for increasing MIMO spatial multiplexing due to antenna size constraints.

In Japan, terminal collaborative technology has been actively studied to solve these issues and realize new use cases. This white paper comprehensively covers these research and development activities and provides an overview of some of them. The structure of this white paper is as follows.

- In Chapter I, the research trends, objectives, and standard models of terminal collaborative technology are explained. It also provides a comprehensive overview of the technical challenges related to each standard model and the literature on their research and development. Additionally, it summarizes the current state of terminal collaborative technology in Japan.

[1] To highlight the importance of joint efforts, this white paper adopts the term *collaborate* as the principal expression.

- In Chapter II, an overview of some research and development cases of terminal collaborative technology is provided, using quantitative evaluation results. It suggests the feasibility of terminal collaborative technology as well as further challenges.

Through this white paper, the feasibility of implementing terminal collaborative and its derivative technologies in mobile communication systems beyond the sixth generation is presented in a comprehensive and relatively easy-to-understand format.

Finally, this white paper was created with the support of many individuals, particularly the contributions of the members of Terminal-Cooperative MIMO Technology Working Group in XGMF 6G Radio Technology Project. We express our gratitude for the contributions of many experts from both industry and academia, and we hope that this white paper will showcase the advanced nature of Japan's research and development to the world.

Terminal-Cooperative MIMO Technology Working Group

Chair

Hidekazu Murata

I. Research Trends in Terminal Collaborative Technology

I-1. Significance of Applying Terminal Collaborative Technology

In recent years, with the rapid increase in traffic in wireless communications, improving data rates has become a significant challenge. To address this issue, from the fifth-generation mobile communication systems (5G) onwards, it has been considered to extensively utilize high-frequency bands such as millimeter-wave and terahertz bands to improve throughput. However, high-frequency waves have strong directivity and significant propagation loss. On the other hand, the Sub-6 band (3.6 GHz - 6 GHz) below 6 GHz, which is advantageous in terms of transmission distance, has also been allocated. However, the bandwidth of this band is limited. Terminal collaborative technology is being studied to realize communication that complements the drawbacks of each by using a combination of the Sub-6 band as well as the millimeter-wave or terahertz bands [1,2]. In terms of recent movements in this research area, terminal collaborative technologies such as user equipment (UE) aggregation [3,4] or UE MIMO collaboration [5,4] have been presented. It is anticipated that similar technologies will be proposed and discussed in various opportunities.

I-2. Standard Models of Terminal Collaborative Technology

Terminal collaborative technology involves multiple terminals collaborating in the Sub-6 band with longer transmission distances, while exchanging transmit and received signals between terminals in the millimeter-wave or terahertz bands with wider frequency bandwidths. The following three forms are considered as standard models.

I-2.1. Downlink Terminal Collaborative MIMO Signal Reception

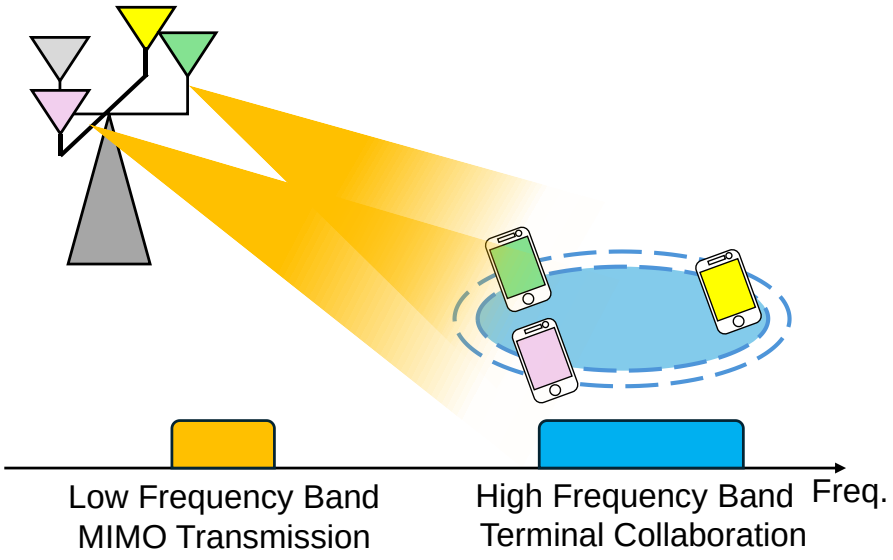

Fig. 1-2-1 Downlink Terminal Collaborative MIMO Signal Reception.

A model diagram of downlink terminal collaborative multi-input multi-output (MIMO) signal reception is shown in Fig. 1-2-1. In this model, the base station simultaneously transmits signals from multiple antennas to each terminal in the low-frequency band. Each terminal receives these signals and exchanges them in the high-frequency band. They work as virtual antenna elements and carry out MIMO signal detection.

I-2.2. Uplink Terminal Collaborative MIMO Signal Transmission

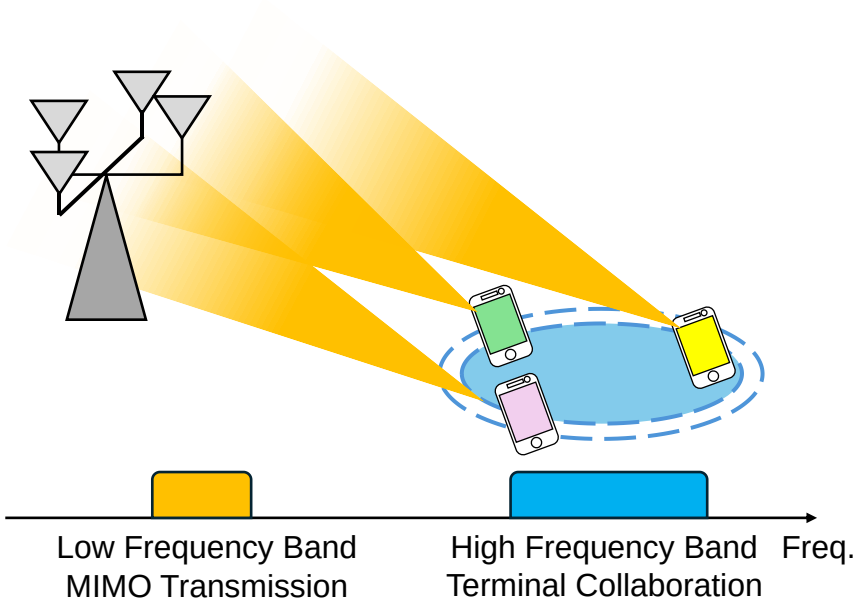

Fig. 1-2-2 Uplink Terminal Collaborative MIMO Signal Transmission.

A model diagram of uplink terminal collaborative MIMO signal transmission is shown in Fig. 1-2-2. In this model, terminals first exchange signals they are going to transmit with each other in the high-frequency band. It is also possible for a specific terminal to request another terminal to transmit a signal on its behalf. In the low-frequency band, multiple terminals simultaneously transmit signals to the base station. The base station receives the signals and performs MIMO signal detection.

I-2.3. Uplink Terminal Collaborative Beamforming Signal Transmission

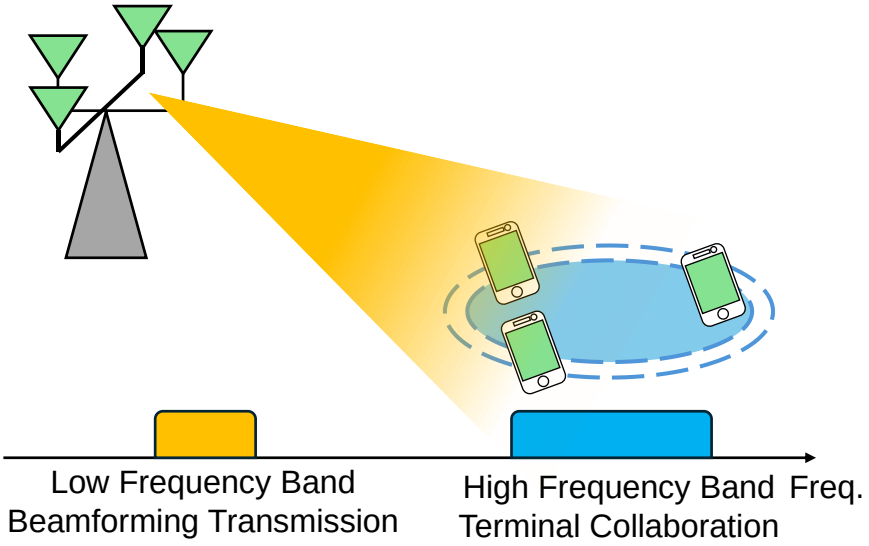

Fig. 1-2-3 Uplink Terminal Collaborative Beamforming Signal Transmission.

A model diagram of uplink terminal collaborative beamforming (BF) signal transmission is shown in Fig. 1-2-3. In this model, a specific terminal assigned to a frequency resource requests the other terminals to transmit a signal on its behalf. In the low-frequency band, multiple terminals simultaneously transmit the signal to the base station. In this case, phase adjustment is applied on the transmit signal so that the signal phases are coherently received at the base station. The base station receives and demodulates the signals.

I-3. Technical Issues in Terminal Collaborative Technology

Terminal collaborative technology has common technical issues that need to be addressed in any of the standard models shown in Section I-2, as well as issues specific to each standard model. An overview of these issues and the latest studies on them are provided in the following.

I-3.1. Common Technical Issues

- Collaborative Processing (Grouping of Devices and Assistants)

  With the cooperation of multiple terminals, it is possible to effectively utilize transmitted signals between them and perform space-division multiplexing in order to achieve successful signal reception. This optimization process results in a higher level of demodulation accuracy and better receiver error rates by selecting optimal received signals for each spatial stream. Additionally, knowing different receiving conditions helps maintain an overall high quality communication link.

The technology of shared terminal groups can be listed as follows:

1. **MMSE interpolation** - The method of selecting a terminal combination pattern using the residual error factor.
2. **signal selection per spatial stream** - a demodulation process that uses a different combination of received signals for each spatial stream.
3. **inter-radio station coordination link generation/update** - autonomous broadcast signaling to generate and update coordination information between radio stations.
4. **dynamic multi-antenna transmission** - multi-antenna transmission based on the coordination state of radio stations under base station control or autonomous control.
5. **calculation of received signal strength information** - calculation relay communication control information based on received signal strength information from terminals。
6. **use of preamble section** - communication management utilizing preamble section including relay information and number of transmitted streams.

These techniques are important to facilitate cooperation among terminals and improve communication quality.

For example, the MMSE equalization iteration technique is a method for effectively processing signals received from multiple terminals in a wireless communication system. The main features and processes of this technique are as follows:

1. **use of residual error coefficients:** minimum mean squared error (MMSE) equalization uses the residual error coefficients obtained in each loop to select the terminal combination pattern. This improves demodulation performance.
2. **improved tolerance:** Conventional methods determine terminal combinations based only on the results of the last loop, which is not sufficiently tolerant of time variations. MMSE equalization iteration, however, takes into account the results of all loops, allowing the selection of terminal combinations that are less sensitive to time variations in the channel.
3. **reduced processing:** Efficient data transmission can be achieved by reducing the amount of processing required while maintaining the same communication quality.
4. **Improved robustness:** This technology improves the quality of communications when the same terminal combination is used continuously, especially in terms of lower frame error rate (FER).

MMSE equalization iteration is an important technique for improving the accuracy of signal processing in wireless communications and providing a stable communication environment.

- Wireless Security
  Technologies to ensure group security in which information can be transmitted only within a group of legitimate user terminals, and eavesdroppers cannot successfully obtain information from communication signals nor falsify data, and to control security authentication, addition, and ejection during group formation and transition [7,8].
- OFDM systems suffer from the problem of phase noise (PN). Channel estimation (CE) and equalization is important to mitigate this problem, and the time window averaging CE for complex time frequency interferometry (CTFI) pilot signal is available in this study [9,10].

I-3.2. Technical Issues in Downlink Terminal Collaborative MIMO Signal Reception

- Access Control
  Exchanging signals among terminals while reducing interference improves the performance of terminal collaborative systems. Access control methods in inter-terminal communications are being studied [11,12].
- Terminal Grouping
  In terminal collaborative MIMO signal reception, the system throughput generally increases as the number of terminals in each group increases. Algorithms for distributed group formation by individual terminals are being studied [13,14].

I-3.3. Technical Issues in Uplink Terminal Collaborative MIMO Signal Transmission

- High-Capacity Data Transmission
  A virtualized terminal combining terahertz and millimeter waves for relay transmission enables high-capacity data transmission [15]. The virtualized terminal consists of a UE, equivalent to a smartphone, and relay devices (RDs), corresponding to wearable devices. To ensure high-capacity wireless connections between the RDs with transferred antenna functions and the UE, the terahertz band is utilized.

I-3.4. Technical Issues in Uplink Terminal Collaborative Beamforming Signal Transmission.

- Terminal Grouping
  In the uplink, the signal of a terminal assigned to a frequency resource is shared among the terminals within the group and the phase of the transmit signal is adjusted to ensure coherent combining at the base station. Terminal groups are formed on a per-terminal basis [16].
- Signal Transfer Processing

The effectiveness of collaborative MIMO transmission is demonstrated from the perspective of effective throughput performance, taking into account the sharing of channel state information and data signals between user terminals [17].

REFERENCES

[1] Y. Hayashi, I. Shubhi, and H. Murata, “User Collaboration for Interference Cancellation on Multi-User MIMO Communication Systems,” IEEE 82nd Vehicular Technology Conference, Sept. 2015.

[2] L.-S. Tsai, S.-L. Shih, P.-K. Liao, and C.-K. Wen, “MIMO Evolution Toward 6G: End-User-Centric Collaborative MIMO,” IEEE Communications Magazine, vol. 62, issue 7, pp. 104-110, July 2024.

[3] RP-242973, CMCC, "Views on UE aggregation for Rel-20," 3GPP RAN #106, Dec. 2024.

[4] RP-243153, ZTE, "Views on UE aggregation for 5G-A in Rel-20," 3GPP RAN #106, Dec. 2024.

[5] 6GWS-250008, ZTE, "6G Motivation and Day1 Functions -RAN Aspects," 3GPP workshop on 6G, March 2025.

[6] 6GWS-250071, Mediatek, "MediaTek Views on 6G Day-1 -Radio Aspects," 3GPP workshop on 6G, March 2025.

[7] K. Ito and E. Okamoto, "Study on Physical-Layer Encrypted Relay Transmission Method Using Group Key for Distributed Terminal Cooperative Communication," IEICE Tech. Rep., vol. 124, no. 84, RCS2024-62, pp. 203-208, June 2024.

[8] N. Horiike, E. Okamoto, and T. Yamamoto, "A downlink non-orthogonal multiple access scheme having physical layer security,” EURASIP Journal on Wireless Communications and Networking, vol. 2018, no. 1, pp. 1-11, Aug. 2018.

[9] S. Okamoto, Y. Ida, Y. Ohira, S. Kuroda, and T. Matsumoto, “Phase noise compensation with time window averaging for WHT-CTFI-OFDM,” 2024 IEEE 13th Global Conference on Consumer Electronics (GCCE2024), pp. 1392–1393, Oct. 2024.

[10] S. Okamoto, Y. Ida, Y. Ohira, S. Kuroda, and T. Matsumoto, “Phase noise compensation with time window averaging for Hadamard spreading CTFI-OFDM,” IEICE Technical Report, CS2024–10, pp. 13-14, July 2024.

[11] Y. Li, H. Okada, and C. Ben Naila, “Evaluation of access control mechanisms within inter-terminal cooperation in millimeter-wave communication systems,” IEICE International Conference on Emerging Technologies for Communications (ICETC), P1-04, 2024.

[12] H. Okada, Y. Li, and C. Ben Naila, “Performance evaluation of mmWave terminal cooperative communications using directional antennas,” IEEE Asia-Pacific Conference on Communications (APCC), pp.290-294, 2024.
[13] E. Ando and Y. Sanada, "Performance of Collaborative MIMO Reception with User Grouping Schemes," IEICE Trans. on Commun., vol. E107-B, no. 1, pp. 253-261, Jan. 2024.
[14] E. Ando and Y. Sanada, "Performance of User Grouping Schemes in Collaborative MIMO Reception with a Focus on User Fairness," IEEE 100th Vehicular Technology Conference, Washington D.C., Oct. 2024.
[15] KDDI corporation, KDDI Research, Inc., “Beyond 5G/6G White Paper ver.2.0.1,” Oct. 2021, https://www.kddi-research.jp/english/tech/whitepaper_b5g_6g/
[16] R. Nakaoka, E. Ando, and Y. Sanada, "Throughput Performance of Uplink Beamforming Transmission through Terminal Collaboration," IEEE 100th Vehicular Technology Conference, Washington D.C., Oct. 2024.
[17] A. Yue, K. Maruta, “Performance Analysis of Collaborative Uplink MIMO Transmission Considering Signaling Overhead,” Proc. ACM Intelligent Computing and its Emerging Applications (ICEA 2024), Tokyo, Japan, November 2024.

II. Recent Advances in Terminal Collaborative Technology in Japan

To achieve the ambitious targets of Beyond 5G/6G, new methods of utilizing frequency resources are essential. Terminal collaborative technology is considered one of the key technologies for achieving the ambitious goals of Beyond 5G/6G. This technology effectively utilizes sub-6 GHz frequency bands while promoting the use of millimeter-wave frequency bands. This chapter addresses the recent advances in terminal collaborative technology in Japan.

II-1. Terminal Collaborative Transmission Project

This section focuses on terminal collaborative transmission projects supported by Grant-in-Aid for Scientific Research (A) under Grant No. 23H00474 from the Ministry of Education, Culture, Sports, Science, and Technology of Japan.

II-1.1. Terminal-Collaborated MIMO Reception

Hidekazu Murata
Yamaguchi University,
Satoshi Suyama
NTT DOCOMO, INC.

Abstract— **In terminal-collaborated multiple-input multiple-output (MIMO) reception, it is essential to appropriately select the terminal that will act as the collaboration partner. In frequency-selective fading channels, transmission performance can be improved by selecting suitable terminals for each frequency subband. To this end, MIMO channel matrix-based schemes have been proposed for subband-level terminal selection. Additionally, residual error coefficients obtained during signal processing have proven to be reliable indicators of decoding performance. This section proposes efficient subband-based terminal selection schemes utilizing a two-stage process based on both MIMO channel matrices and residual error coefficients, aiming to further enhance subband-based terminal selection performance. The proposed schemes were evaluated using both computer simulations and real-world signal measurements. The results confirm that the proposed approach outperforms conventional methods in terms of transmission performance.**

II-1.1.1. Introduction

In MIMO transmission systems, channel capacity is constrained by the lesser number of antennas on either the transmitter or receiver side. Although significantly increasing the number of antennas in a small terminal is challenging, the equivalent number of receive antennas can be increased by leveraging collaboration among neighboring terminals.

In terminal-collaborated MIMO reception [1], this equivalent expansion is achieved through joint reception of MIMO signals from the base station (BS) by multiple terminals. High-frequency communication technologies, such as those in the 28 GHz band, are particularly well-suited for establishing collaborative links due to their support for high-speed and low-latency transmission.

To reduce the overhead associated with collaboration, terminal selection is employed to identify suitable receiving terminals. Various schemes have been proposed, including those based on the MIMO channel matrix and those utilizing residual error coefficients as selection metrics.

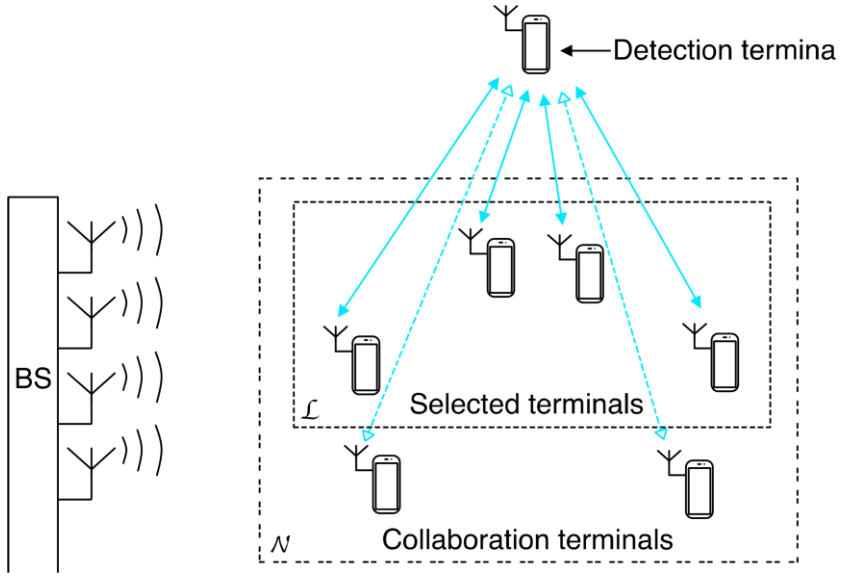

Fig. II-1.1-1 System model of terminal-collaborated MIMO reception.

In multipath fading environments, where delay spreads are present, frequency-selective fading causes the channel state to vary across frequency subbands. Thus, subband-level adaptive terminal selection becomes desirable. Prior work has demonstrated that subband-based selection using channel matrix properties enhances performance as the number of subbands increases [2]. Additionally, residual error coefficients provide a strong indication of decoding performance but introduce computational complexity since decoding must be attempted during selection.

This section introduces a two-stage terminal selection approach: the first stage employs channel matrix-based selection to narrow the candidate terminals, and the second stage utilizes residual error coefficients to further refine selection [3]. The signal processing assumes frequency-domain iterative equalization using a minimum mean squared error (MMSE) filter.

II-1.1.2. System Model

This section introduces the system model and frequency-domain iterative equalization process. Fig. II-1.1-1 depicts the system model for collaborative terminal selection in a terminal-collaborated MIMO reception scenario. Each terminal is equipped with a single antenna, and multiple independent signals are transmitted simultaneously from the BS to the terminals over the same frequency band. First, the detection terminal collects only the necessary portions of received signals (e.g., for channel estimation) from the

collaborating terminals and then performs decoding using the other necessary portions of the received signals.

II-1.1.3. Subband-based signal processing and performance

The transmission performance of the proposed method was evaluated via computer simulations and actual received signals, focusing on the number of subbands and signal-to-noise ratio (SNR). Frequency-domain soft cancellation and MMSE-based iterative equalization were employed for terminal-collaborated MIMO reception. Fig. II-1.1-2 shows a block diagram of the proposed subband-based terminal selection and equalization method, assuming four BS antennas and six receiving terminals.

Each terminal performs a discrete Fourier transform (DFT) to convert the received signal to the frequency domain. The subband-specific portions of these signals are forwarded to the detection terminal via high-frequency communication links. The detection terminal performs frequency-domain iterative equalization using the collected signals.

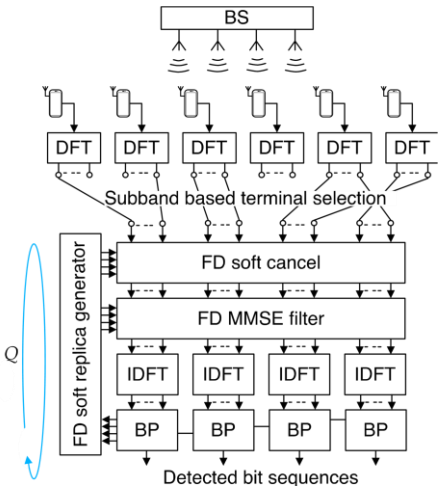

Fig. II-1.1-2 Subband-based terminal selection and iterative equalization.

Fig. II-1.1-3 presents the packet error rate (PER) performance as a function of the number of subband divisions, S, for various terminal selection algorithms. The best performance was achieved by the SIMPMC scheme, which selects terminals based on signal-to-interference-plus-noise ratio (SINR), singular values, and condition number of the MIMO channel matrix. Compared to the conventional $S = 1$ scheme that selects terminals across the full bandwidth, the proposed subband-specific selection achieves approximately an order of magnitude improvement in PER.

To validate the proposed schemes in real environments, offline processing was performed using recorded signals from an actual outdoor 4×6 MIMO transmission experiment [3]. Fig. II-1.1-4 illustrates the experimental setup, which includes a 4-channel software-defined radio (SDR) transmitter at the BS and six SDR-based MS receivers, all managed via PC control. The MS-side signals were recorded via Gigabit Ethernet (GbE) and used for subsequent processing.

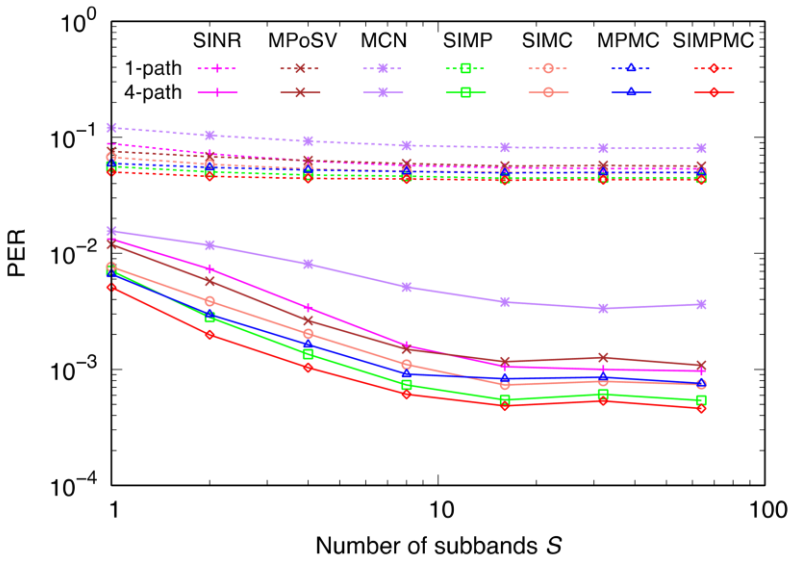

Fig. II-1.1-3 Packet error performance versus number of subbands.

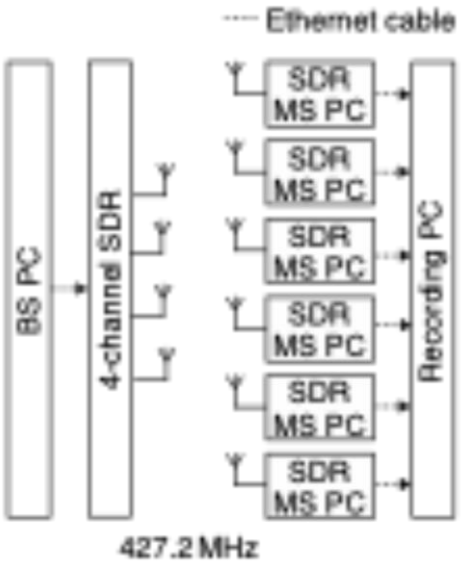

Fig. II-1.1-4 MIMO 4x6 experiment system.

Fig. II-1.1-5 Experimental field.

Fig. II-1.1-5 shows the experimental environment. The BS was mounted on the rooftop of a 31-meter-high building, and the six MSs were arranged on a circle with a 4-meter radius, located 143 meters from the BS. The MSs were connected to the recording PC via

GbE. During measurement, the MSs moved counterclockwise around the circle at approximately 2 km/h while maintaining their relative positions. The signal reception was performed twice under identical conditions using frequency-domain iterative equalization.

This study also investigates the SINR+1MS scheme, which extends the SINR-based selection by adding one extra MS based on residual error coefficients. Fig. II-1.1-6 shows

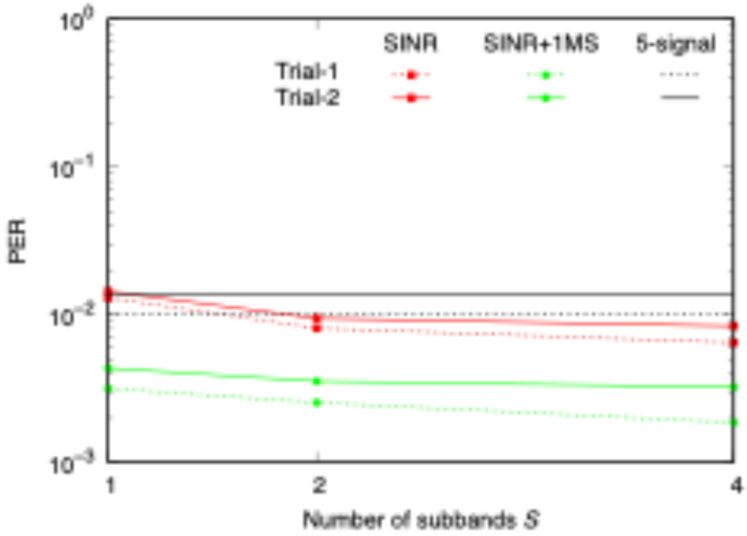

Fig. II-1.1-6 PER performance using actual received signals.

the PER performance versus the number of subband divisions S for SINR+1MS, comparing it to the original SINR scheme and a 5-fixed-terminal scheme. In both experimental trials, SINR+1MS consistently outperformed the baseline methods in PER.

II-1.1.4. Conclusion

This section proposed a two-stage subband-based terminal selection scheme for terminal-collaborated MIMO reception. The approach combines channel matrix-based selection and residual error coefficient-based refinement to enhance transmission performance while minimizing decoding complexity. Experimental and simulation results confirm that the proposed method achieves superior error performance compared to conventional single-stage selection approaches.

REFERENCE

[1] F. Du, H. Murata, M. Kasai, T. Nakahira, K. Ishihara, M. Sasaki and T. Moriyama "Distributed detection of MIMO spatial multiplexed signals in terminal collaborated reception," IEICE Trans. Commun., vol. E104.B, no. 7, pp. 884-892, July 2020.

[2] H. Murata, “Terminal selection schemes in terminal-collaborated MIMO reception based on subband channel matrices,” IEEE Communications Letters, vol. 26, no. 1, pp. 202-206, Jan. 2022.
[3] R. Kanda, H. Murata, X. Du, S. Suyama, H. Jiang, “Performance of MIMO reception technique with adaptive terminal selection in each sub-band using actual received signals,” ITE Technical Report, BCT2025-36, pp. 38-41, Feb. 2025.

II-1.2. Filter-and-Forward Collaborative Relaying For Higher Spectrum Efficiency

Satoshi Denno

Okayama University, Japan

Abstract— **Filter-and-forward collaborative relaying is proposed in this work for higher spectrum efficiency. The proposed filter-and-forward collaborative relaying needs only two time slots to send a packet to the destination terminal despite of the number of the relays. In addition, because the proposed relaying is regarded as modification of amply-and-forward (AF) relaying, the proposed relaying can be implemented with small computational complexity. Furthermore, distributed relay selection is proposed for the filter-and-forward collaborative relaying. The signal distortion caused by the Doppler shift is taken into account in the relay selection. Computer simulations show that the filter-and-forward collaborative relaying achieves superior transmission performance even in double selective fading channels.**

II-1.2.1. Introduction

The 5G evolution and 6G system are planned to provide users higher speed communication links than the 5G system, which is expected to raise the network throughput. While many techniques have been proposed [1,2], the collaborative relaying is one of those techniques [3]. The collaborative relaying makes use of neighboring cell phones as relays, which forward the received signals to the destination terminal for improving communication quality and communication speed. While relaying is known to improve the transmission performance at cost of spectrum efficiency, the collaborative relaying alleviates the problem of the low spectrum efficiency by using higher frequency bands for forwarding the signals from relays to the destination terminal in downlinks. In uplinks, the terminal sends the signal for the relays in higher frequency bands. However, spectrum efficiency possibly reduces as the number of the relays increases. On the other hand, when some of the relays move so fast, the collaborative relay is degraded by them, even if they are located near by the terminal.

This work proposes new collaborative relaying which is named as “Filter-and-Forward collaborative relaying”. The proposed filter-and-forward collaborative relaying achieves higher spectrum efficiency, because the proposed relaying can send the signal to the destination terminal via relays in two time slots despite of the number of the relays. Furthermore, the proposed collaborative relaying achieves higher diversity gain as the number of the relays increases, because the proposed collaborative relaying has a functionality to select the best combination of the relays based on the signal to noise power ratio where the Doppler shift is also taken into account. In addition, we propose

distributed relay selection for the proposed collaborative relaying, which makes it easier to implement the collaborative relaying in real wireless communication environment.

II-1.2.2. Configuration of Proposed Filter-and-Forward Collaborative Relaying

A base station sends a packet in a microwave band for the terminals, some of which play a role of relay except for the destination terminal in the collaborative relaying. The orthogonal frequency division multiplex (OFDM) is applied to the packet. The packet is received and is filtered based on the MMSE criterion in the frequency domain at the relays. In parallel with the signal transmission, the destination terminal sends a packet to the relays in a higher frequency band for the relay to estimate the channel. Also, the channel impulse response between the relay and the base station is estimated at the relay, simultaneously. Those estimated channel impulse responses are utilized for the MMSE-based filtering. The above signal processing is performed in the first time slot. The filtered packet is forwarded to the destination terminal in the higher band and received at the terminal. The received signal is fed to the region detection to demodulate the signals in the second slot. As is described above, the collaborative relaying is finished in the two slots. The configuration is shown in Fig. II-1.2-1. As is shown in the figure, the received signal is a superposition of the filtered signals sent from the relays. However, since the filtering at the relays is regarded as a kind of precoding, the signals are almost co-phased when they are received at the terminal. This is the reason why the signal detection gets simple as described above.

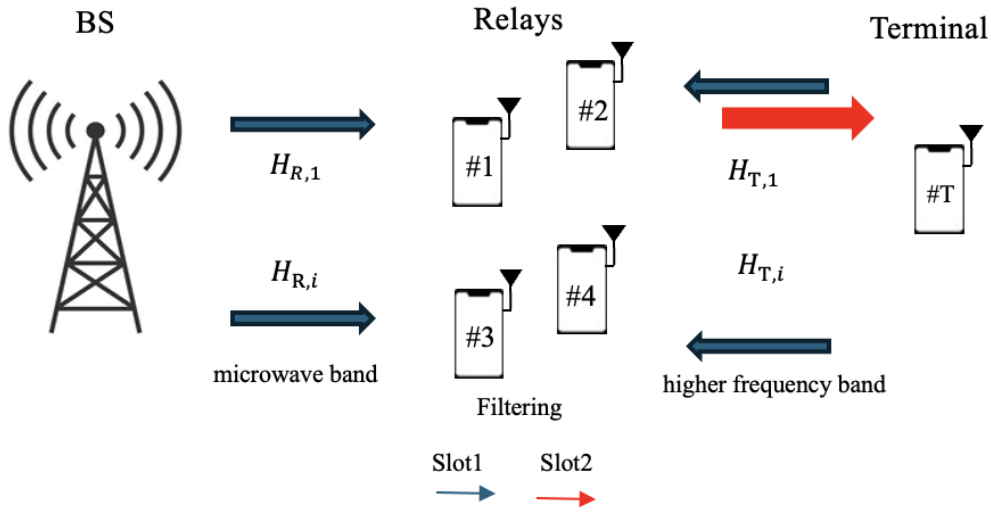

Figure II-1.2-1 System configuration of filter-and-forward collaborative relaying.

II-1.2.3. Signal to Noise Power Ratio Estimation at Destination Terminal

As is well known, systems with the OFDM are deteriorated in double selective fading channels. Since this is one of very important issues, many techniques have been

proposed. Because they are sophisticated, however, most techniques impose high computational burden on receivers. Since the terminals play a role of the relay, such sophisticated techniques can't be applied to not only the relays but also the destination terminal. Instead, only the signal-to-noise power ratio (SNR) at the destination terminal is estimated and the SNR is utilized for the relay selection. Because the proposed filter-and-forward collaborative relaying is regarded as a sort of the amplify-and-forward relaying, the relays forward not only the signals but also the additive white Gaussian noise (AWGN) generated at the relays to the destination terminal. The AWGN forwarded from the relays is mixed with that generated at the destination terminal, which behaves as the AWGN at the terminal. On the other hand, the received signal at the destination terminal is influenced by the Doppler shift caused by the movement of the relays. The proposed collaborative relaying estimates the Doppler shift in a packet, and predicts the signal distortion in a packet owing to the Doppler shift. The distortion is taken into account in the SNR estimation as well as the AWGN. On the other hand, the signals sent from all the relays are combined coherently at the destination terminal with assistance of the filters at the relays. This is the reason why the proposed collaborative relaying achieves higher diversity gain as the number of the relays increases.

II-1.2.4. Relay Section

There can be many terminals concentrated around the destination terminal, and some of them move so fast. We should select relays that contribute transmission performance improvement in the proposed collaborative relaying [4]. The SNR defined above is applied to the selection of the relays. The relays far from the destination terminal and those moving so fact can be excluded from the relays forwarding the packet. However, the channel impulse responses between the base station and the relay, and that between the relays and the destination terminal need to be collected to calculate the SNR, which requires additional transaction between the terminal and the relays. We propose a distributed relay selection technique that allows each relay to determine by itself whether it should forward the received signal or not.

II-1.2.5. Computer Simulation

The performance of the proposed filter-and-forward collaborative relaying is evaluated by computer simulation. The relays move around the destination terminal, while the base station transmits a packet at a distance. The velocity of the relays is uniformly distributed from 0 km/h and $V_{\max}$ km/h. The base station sends the packet in 3 GHz and the relays forward the packet in 30 GHz. The SNR performance of the proposed collaborative relaying is shown in Figure II-1.2-2, when the relays are selected based on

the SNR. The three relays are selected at most in the figure. The vertical axis is the SNR at the terminal and the horizontal axis is the maximum velocity $V_{\max}$. While the dotted line shows the performance of the random selection, the solid lines are the performances of the proposed selection. The proposed selection achieves better SNR performance even when there are only three terminals. The SNR performance is improved as the number of the relays increases.

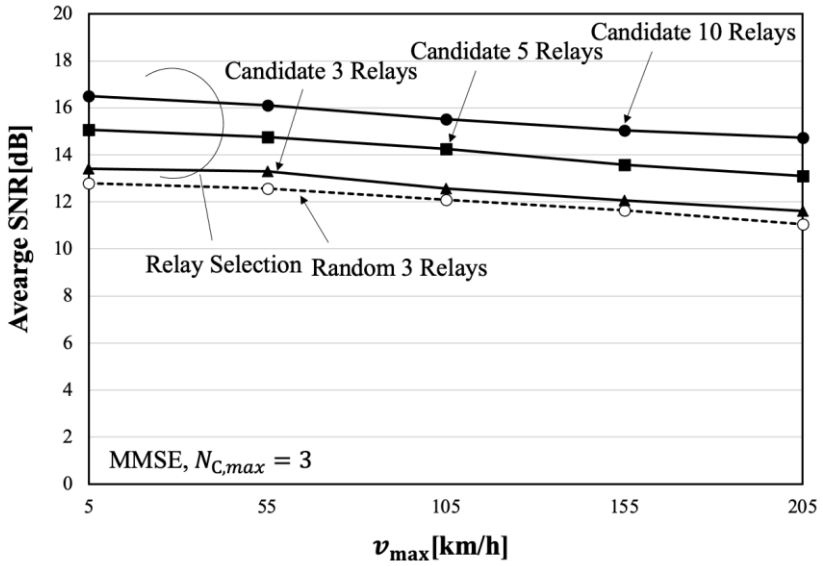

Figure II-1.2-2 theoretical relay selection in the proposed relaying.

Figure II-1.2-3 shows the SNR performance of the proposed filter-and-forward collaborative relaying when the proposed distributed relay selection is applied. The same fading channel to that in Fig. II-1.2-2 is applied. The number of the relays is set to 5 in the figure. The threshold to determin whether the relay forward the packet or not, is changed from 5 dB to 7.5 dB. The maximum SNR indicates the perfomance of the filter-and-forward collaborative relaying with the SNR-based relay selection explained in the previous section. In addition, the performance of the relaying with random selection is drawn as a reference. The proposed disitributed relay selection with the threshold of 7.5 dB enables the proposed filter-and-forward collaborative relaying to achieve as superior performance as the SNR-based relay selection. The proposed relay selection attais much better SNR performance than the random selection.

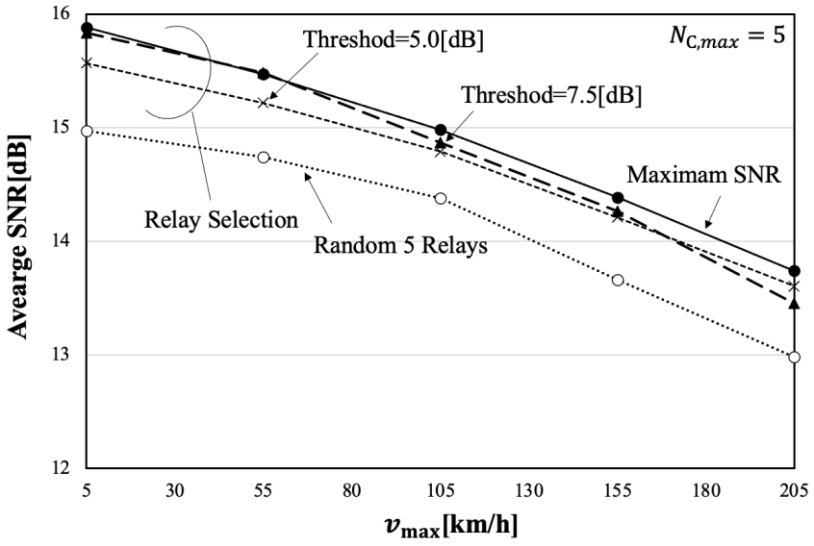

Figure II-1.2-3 the SNR performance of the proposed relay selection.

II-1.2.6. Conclusion

Filter-and-forward collaborative relaying has been proposed for high spectrum efficiency. In fact, only two time slots are necessary to send a packet to the destination terminal from the base station via relays. Reley selection based on the SNR for the relaying has been proposed. Furthermore, distributed reley selection has also been proposed. The superiort performance is confired by computer simulation. The proposed filter-and-forward collaborative relaying with SNR-based relay selection achieves better SNR performance than that with random selection in double selective fading channel. The propsed distibuted relay selection enables the proposed collaborative ralaying to improve the transmission performance in the fading channel, as long as the selection threshold is set appropriately.

REFERENCE

[1] M. Shafi, A. F. Molisch, P. J. Smith, T. Haustein, P. Zhu, and P. D. Silva "A Tutorial Overview of Standards, Trials, Challenges, Deployment, and Practice," IEEE Journal on Selected Areas in Communications, vol.35, no. 6, pp.1201-1221, 2017.

[2] L. Sanguinetti, A. A. D'Amico, and Y. Rong "A Tutorial on the Optimization of Amplify-and-Forward MIMO Relay Systems," IEEE Journal on Selected Areas in Communications, vol.30, no. 8, pp.1331-1346, 2012.

[3] H. Murata, "Terminal Selection Schemes in Terminal-Collaborated MIMO Reception Based on Subband Channel Matrices," IEEE Communications Letters, vol.26, no.1, pp.202-206, 2022.

[4] S. Denno, T. Fujii, and Y. Hou “Adaptive Collaborative Relaying in High Mobility Environment,” 25th International Symposium on Wireless Personal Multimedia Communications (WPMC), 2022.

II-1.3. Wireless Security for Terminal Collaborative Communication System

Eiji Okamoto and Keita Ito
Nagoya Institute of Technology

Abstract— **In a mobile terminal, implementing a large number of antennas is difficult, and, it is effective to develop the terminal collaborative communication system, in which virtual multiple-input multiple-output (MIMO) transmission is realized by cooperative communication among neighboring mobile terminals and the capacity is expanded. Moreover, the security of wireless communication has been a concern in recent years. However, there have been insufficient studies on techniques to ensure the confidentiality in terminal cooperative communication system (TCCS). In this section, we propose a physical layer-encrypted terminal cooperative communication system based on a chaos modulation scheme using a group key, and show that both physical layer confidentiality in the group and communication quality improvement can be achieved through numerical simulations.**

II-1.3.1. Introduction

With the spread of wireless communication terminals, the frequency of Internet service and content usage through various devices is increasing. In this trend, opportunities to exchange personal information, such as for online banking and credit card payments, are also increasing. According to a survey, 90% of Internet users are concerned about "leakage of personal information and Internet usage history," and it is an important issue to improve the confidentiality of wireless communications, such as defense measures against information leakage and eavesdropping to third parties [1]. To meet this demand, we have proposed a radio-encrypted modulation scheme called chaos-multiple-input multiple-output (C-MIMO) transmission based on chaos communication [2,3]. This system applies chaos modulation to MIMO block transmission. C-MIMO transmission scheme modulates by convolution of transmitted bits to obtain the effect of channel coding with a coding rate of 1, while at the same time providing physical layer security through radio wave encryption by chaotic signals. By sharing the initial value of chaos as a key signal between the transmitting and receiving sides, a third party who does not have the chaos key will not be able to decode even a small discrepancy in the key. Compared to conventional upper-layer security techniques, the method of ensuring security at the physical layer simplifies the security protocol, thereby improving communication efficiency and reducing power consumption. It can also be used in combination with upper-layer security technologies to enhance security.

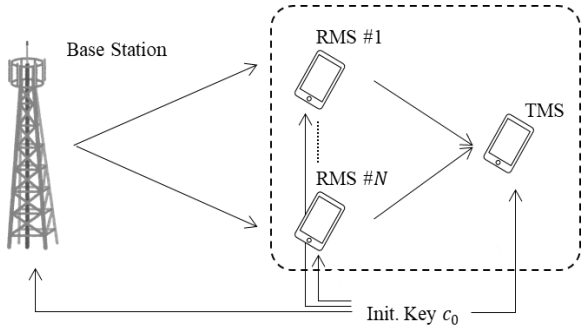

Fig. II-1.3-1 Downlink terminal collaborative communication system.

In terminal collaborative communication system (TCCS) [4], there is a risk that an eavesdropper who enters a virtual antenna arrays (VAA) cell composed of a group of cooperating terminals may intercept signals from base stations or relay terminals, resulting in loss of confidentiality of communication. To prevent this, there have been few studies on how to ensure security in terminal collaborative communication, and most of them are based on the assumption that upper-layer authentication and scrambling used in existing 5G cellular systems are used to ensure confidentiality. Although some techniques have been proposed to ensure physical layer security in 5G and Beyond 5G [5,6], there has been little research on physical layer security of communications in TCCS.

In this section, we consider the application of chaos modulation to TCCS and propose a transmission scheme with group security that has a common key among base stations and cooperating terminals. We evaluate its transmission characteristics and communication confidentiality [7].

II-1.3.2. Terminal Cooperative Communication System Applying Chaos Modulation Scheme

A half-duplex decode-and-forward (DF) relay transmission using relay terminals is discussed. Fig. II-1.3-1 shows a system model of downlink MIMO communication with terminal coordination. We consider that a data signal is sent from a base station (BS) to a certain final receiving terminal, target mobile station (TMS), and is transmitted through N relay terminals, named relay mobile stations (RMS). The communication between BS and RMS is assumed to be in sub-6 bands, and is affected by propagation path fluctuations and additive white Gaussian noise (AWGN). In contrast, for communications between terminals, assuming that the terminals are in close proximity and the relative position changes are small, and assuming the use of high frequency bands such as the extra high frequency (EHF) band, it is considered that only the effect of AWGN should be considered. In the C-MIMO transmission system, the initial chaos

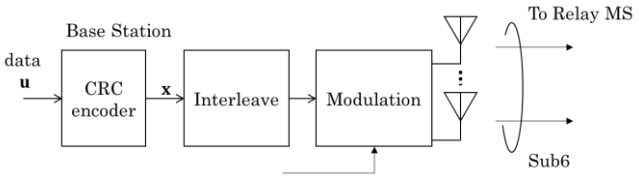

Fig. II-1.3-2 Configuration of base station for terminal coordination and cooperative communication system.

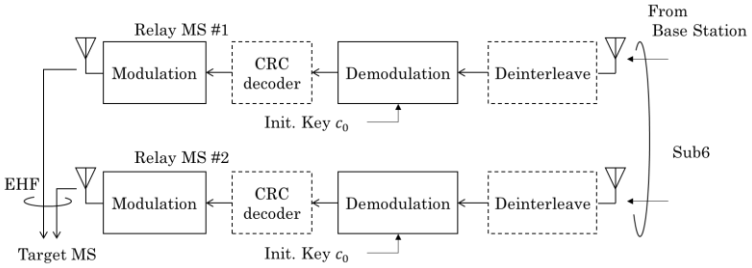

Fig. II-1.3-3 Configuration of relay terminals for terminal coordination and cooperative communication system.

value $c_0 \in \mathbb{C}$ is used as a common key by the transmitter and receiver. Therefore, BS, RMS, and TMS share this common key c_0. The group key sharing method is assumed to be pre-distributed by BS. Specific protocols to control security authentication, addition, and egress at the time of specific group formation are a topic for future study.

Fig. II-1.3-2 shows the structure of a transmitter at a BS. First, a codeword obtained by cyclic redundancy check (CRC) code is assigned to the information word series to be transmitted, and one packet of the series consisting of this CRC and codeword is modulated and transmitted. In chaos modulation, the transmitted bits are correlated so that they are convolved during modulation to generate a series of modulated symbols, and interleaving is performed within the packet to reduce the effect of channel correlation between symbols. However, because maximum likelihood sequence estimation (MLSE) is used to demodulate chaotically modulated signals, the amount of demodulation operations increases in proportion to a power of 2. To reduce the amount of operations on the demodulation side, a packet is divided into chaotic modulation blocks of $N_t B$ bits each, and each series is modulated as $\mathbf{x}_{Bi} \in \mathbb{C}$ and sent to the RMSs. Here, the received signal $\mathbf{y}_{Ri} \in \mathbb{C}$ at RMS $\#\, i$ is obtained by

$$\mathbf{y_{Ri}} = \mathbf{h}_{Ri}\mathbf{x}_{Bi} + \mathbf{n}_{Ri}, \tag{1}$$

where $\mathbf{h}_{Ri} \in \mathbb{C}$ and $\mathbf{n}_{Ri} \in \mathbb{C}$ are the communication channel matrix between the base station and RMS $\#\, i$ and the received noise signal, respectively, satisfying $1 \leq i \leq N$.

The receiver and transmitter configurations in RMS are shown in Fig. II-1.3-3. In RMS # i, the received signal is demodulated once and error detection is performed by CRC.

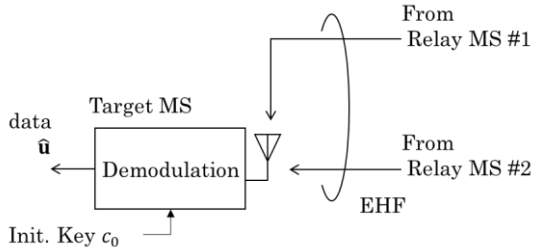

Fig. II-1.3-4 Configuration of final receiving terminal for terminal cooperative communication system.

Table II-1-3-1 Simulation configurations

Modulation	Chaos (proposed)	BPSK
Chaos Block Length NtB	4, 6	—
Number of Chaos Iteration	100	—
Packet Length N	48	
Number of Transmission Antenna at BS N_t	2	
Number of Received Antenna at MS N_r	1	
Number of RMSs	2	
BS – RMS channel	1 pass symbol i.i.d. quasi-static Rayleigh fading + AWGN SNR: 25 dB fixed	
Channel Estimation	Perfect	
RMS – TMS channel	AWGN	

The demodulated signal is modulated again in RMS, multiplied by the power factor α_i as

$$\alpha = \begin{cases} 1/\sqrt{N} & if \text{ No Error} \\ 0 & if \text{ Error} \end{cases} \quad (21)$$

and transmitted.

Finally, the received signal $\mathbf{y}_T$ in TMS is obtained by

$$\mathbf{y}_T = \sum_{i=1}^{N} \alpha_i \mathbf{x}_{Ri} + \mathbf{n}_T, \quad (3)$$

where $\mathbf{x}_{R_i}$ is the transmitted signal from RMS # i and $\mathbf{n}_T$ is the received noise power at TMS. As shown in Fig. II-1.3-4, TMS performs chaos demodulation to obtain the information bit series. By setting a power factor α_i based on the CRC result in RMS, inter-symbol interference in TMS can be prevented because RMS does not receive error-detected packets. However, the spatial diversity effect of cooperative communication is maximized when no errors are detected in all RMSs.

II-1.3.3. Numerical results

II-1.3.3.1. Packet error rate performance

TCCS was constructed by numerical simulation, and the packet error rate (PER) was calculated. The simulation parameters are shown in Table II-1-3-1. In the transmission

model in Fig. II-1.3-4, the CRC detection indicated by the dashed lines is assumed perfect, and the interleaving is omitted in this simulation because the propagation path variation is assumed to be independent between symbols.

Chaos modulation with one bit per symbol transmission efficiency, i.e., BPSK equivalent, was applied to the modulation part, while BPSK modulation, a non-encrypted transmission, was applied to the comparison part. The number of chaos progressions in chaos modulation was fixed at the initial value $I_0 = 100$. The propagation path between BS and RMS is subject to independent one-wave Rayleigh fading and AWGN for each symbol on each antenna, but the channel information is assumed to be completely obtained at RMS. In contrast, as mentioned above, the channel between RMSs and TMS was assumed to be affected only by AWGN.

The signal-to-noise ratio (SNR) between BS and RMS was fixed, and the SNR between RMS and TMS was varied in the numerical simulations. Fig. II-1.3-5 shows the PER characteristics when the average SNR between the base station and RMS is 25 dB. In the legend, "PC" (power control) refers to the aforementioned power control in RMS, and "Unsync." refers to the user who does not share the initial chaotic key c_0 with the transmitter, i.e., the "Unsync." refers to an eavesdropper. The results show that the PER of eavesdropper is 1.0, and it can be confirmed that the data is not demodulated correctly. This is due to the physical layer confidentiality of chaos modulation, which means that this system has physical layer security within the group of BS, RMSs and TMS. Comparing the results of BPSK modulation and chaos modulation, the PER characteristics are improved for both chaos block lengths $NtB = 4$ and 6 compared to

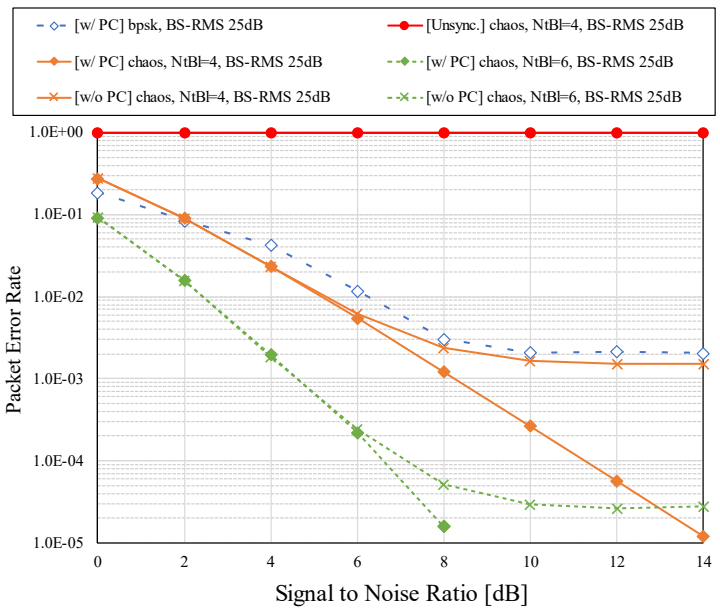

Fig. II-1.3-5 Packet error rate performance when SNR between BS and RMSs is fixed at 25dB.

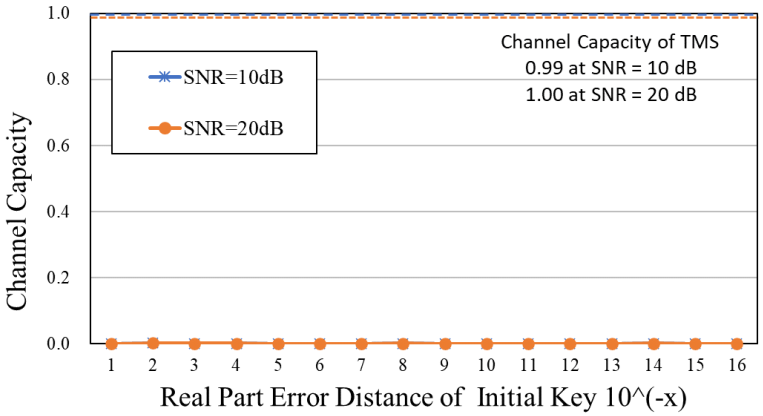

Fig. II-1.3-6 Channel capacity at eavesdropper versus proximity of initial key.

BPSK modulation. This is owing to the coding effect of the chaos modulation with a coding rate of 1. Comparing the results with and without power control in RMS, the "w/o PC" results show an error floor, while the "w/ PC" results show no error floor. This is because the RMS does not send packets containing errors due to CRC checks, which eliminates symbol interference in the signal received by the TMS.

II-1.3.3.1. Secrecy capacity of communication

Subsequently, assuming an eavesdropper intercepting signals from RMS, its secrecy is evaluated from the communication secrecy capacity. In general, the security of wireless communication is evaluated from the viewpoints of information-theoretic security and computational security, and in particular, the information-theoretic security is evaluated in terms of the communication channel capacity of the eavesdropper [8]. The AWGN communication channel is treated as a binary symmetric channel model as an equivalent communication channel, and the channel capacity C_e of eavesdropper is then given by

$$C_e = N_r(1 + P_e \log_2 P_e + (1 - P_e) \log_2 (1 - P_e)), \quad (5)$$

where P_e is the bit error rate of eavesdropper, and the closer the eavesdropper's channel capacity C_e is to 0, the more secure it is [9]. Here, we calculated the channel capacity when an eavesdropper with a key whose real part only deviates by 10^{-x} from the legitimate chaos key shared by BS, RMS, and TMS intercepts a transmission signal from the BS and demodulates it using the deviated key, where x is a positive integer. The simulation parameters are shown in Table 1, but the SNR between BS and RMS was set to 20 dB, and the SNR between RMS and TMS was fixed at 10 dB or 20 dB.

The results show that the legitimate TMS has a channel capacity of about 1.0 at any SNR, while the eavesdropper's channel capacity is almost zero, even at a key difference of 10^{-16}, a resolution that can be checked in the C language. In other words, in order for

an eavesdropper to accurately demodulate a signal transmitted by chaotic modulation, it is necessary to perform a full search with a resolution of 10^{-16} for both the real and imaginary parts of the shared key, and all of the searches must match the legitimate shared key. In other words, the number of decryption operations for an eavesdropper is 10^{32} ($\approx 2^{106}$), confirming that the transmission system has more than 106–bit security from a computational security perspective.

II-1.3.4. Summary

In this section, we proposed a method of applying chaos modulation to TCCS, which is a virtual MIMO transmission technology in which neighboring terminals in a terminal group cooperate to transmit and receive signals from a BS as a relay station, in order to ensure group security by defining the BS, relay terminals and final receiving terminal as one legitimate group. It was confirmed that the proposed method provides physical layer security while improving PER characteristics compared to existing non-confidential transmission systems. We also evaluated the information-theoretic and computational security of the system, and confirmed that the system has physical layer security with a resolution of 10^{-16}, and that it has more than 106-bit security.

REFERENCE

[1] ITU-R Rec. M.2160-0, “Framework and overall objectives of the future development of IMT for 2030 and beyond”, Nov. 2023.

[2] E. Okamoto, “A chaos MIMO transmission scheme for channel coding and physical-layer security,” IEICE Trans. Commun. vol. E95-B, no.4, pp.1384-1392. Apr. 2012.

[3] N. Horiike, E. Okamoto, and T. Yamamoto, "A downlink non-orthogonal multiple access scheme having physical layer security,” EURASIP Journal on Wireless Communications and Networking, vol. 2018, no. 1, pp. 1-11, Aug. 2018.

[4] H. Murata, Akihiro Kuwabara, Yuji Oishi, “Distributed cooperative relaying based on space-time block code: System description and measurement campaign,” IEEE Access, vol. 9,pp.25623-25631, Feb. 2021.

[5] L. Mucchi, S. Jayousi, S. Caputo, E. Panayirci, S. Shahabuddin, and J. Bechtold, "Physical-Layer Security in 6G Networks," IEEE Open Journal of the Communications Society, vol. 2, pp. 1901-1914, Aug. 2021.

[6] P. Devi, M. R. Bharti, and D. Gautam, "A survey on physical layer security for 5G/6G communications over different fading channels: Approaches, challenges, and future directions," Vehicular Communications, vol 53, 100891, June 2025.

[7] K. Ito and E. Okamoto, "Study on Physical-Layer Encrypted Relay Transmission Method Using Group Key for Distributed Terminal Cooperative Communication," IEICE Tech. Rep., vol. 124, no. 84, RCS2024-62, pp. 203-208, June 2024.

[8] F. Oggier, B. Hassibi, “The secrecy capacity of the MIMO wiretap channel,” Proc. Int’l Sym. On Information Theory, pp. 524-528, July 2008.

II-1.4. Phase Noise Compensation with Time Window Averaging for CTFI-OFDM

Shumpei Okamoto, Yuta Ida
Yamaguchi University

Abstract— **Orthogonal frequency division multiplexing (OFDM) is widely utilized in current wireless communications. However, OFDM systems suffer from the problem of phase noise (PN). PN arises due to the multiplication of waves with different carrier frequencies. To solve this problem, we utilize the frequency symbol spreading (FSS) and the complex time frequency interferometry (CTFI) pilot signal. FSS is achieved simply by using Walsh Hadamard transform (WHT). Moreover, CTFI is enhanced to improve the accuracy of channel estimation (CE). However, the problem of PN has not been evaluated for CTFI-OFDM systems. Therefore, in this study, we introduce the PN compensation with the time window averaging for WHT-CTFI-OFDM systems. From the computer simulation results, the proposed method shows about 1.5 dB gain compared to the conventional method.**

II-1.4.1. Introduction

Orthogonal frequency division multiplexing (OFDM) is widely utilized in current wireless communications, and it is expected to play a major role in mobile communications and wireless local area network (WLAN) [1]. However, OFDM systems suffer from the problem of phase noise (PN) [2][3]. PN arises due to the multiplication of the waves with different carrier frequencies when the local oscillator is not synchronized with the carrier frequency. As a result, the system performance deteriorates due to common phase error (CPE) and inter-carrier interference (ICI). Especially in the 5th generation (5G) standard, since high frequency bands such as millimeter waves are utilized, the issue of the PN becomes even more significant [4].

To solve this problem, the equalization such as zero-forcing (ZF) and minimum mean square error (MMSE) is effective. Moreover, in this study, we utilize the frequency symbol spreading (FSS) and the complex time frequency interferometry (CTFI) pilot signal [5][6]. FSS is achieved by Walsh Hadamard transform (WHT) and discrete Fourier transform (DFT). In this study, we utilize the WHT which is achieved simply compared with the DFT. Moreover, CTFI is a kind of pilot signal. CTFI is a cyclic sequence of "1" and "j", and it is improved for the accuracy of channel estimation (CE) by the several time windows averaging, where j is an imaginary. On the other hand, the problem of the PN is not evaluated for CTFI-OFDM system.

Therefore, in this study, we introduce the PN compensation with the time window averaging for CTFI-OFDM systems [7]. From the computer simulation results, the proposed method shows about 1.5 dB gain compared to the conventional method.

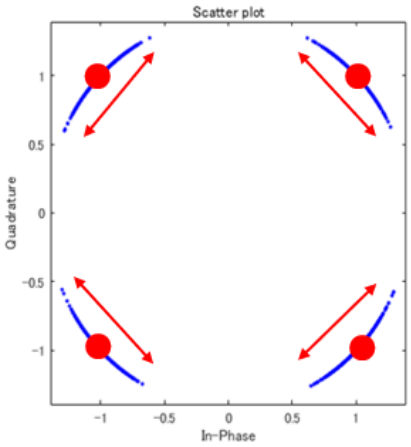

(a) Phase fluctuation.

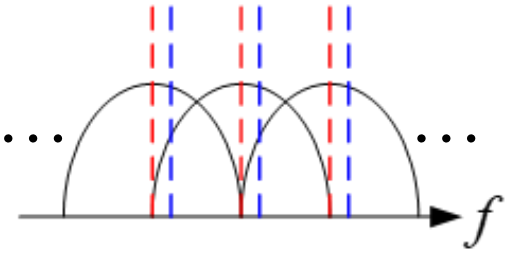

(b) ICI.

Fig. II-1.4-1. Influence of PN.

II-1.4.2. System Model

In this study, at the transmitter, the original signal is generated and coded with interleaving. After the serial-to-parallel (S/P) conversion, the coded signal is modulated by quadrature-phase shift keying (QPSK). Since the proposed method adapts the FSS, the transmitted signal is spread based on WHT as

$$G_{2q} = \begin{bmatrix} G_{2q-1} & G_{2q-1} \\ G_{2q-1} & -G_{2q-1} \end{bmatrix} \quad \text{for} \quad q = 1, 2, 3, \cdots, \tag{1}$$

where $G_1 = 1$. After the WHT spreading, the pilot signal is inserted at the beginning of the packet. Here, the CTFI pilot signal consists of $\{x(k)\} = \{1, j, 1, -j, \ldots, 1, j, 1, -j\}$. Then, after the inverse fast Fourier transform (IFFT), guard interval (GI) is inserted, and the parallel-to-serial (P/S) conversion is performed.

At the receiver, the time domain signal is received. In this study, we assume that PN is only added at the receiver. After the S/P conversion and the GI elimination, the frequency domain signal is obtained by FFT. Here, the received signal of the kth subcarrier in the frequency domain is given by

$$y(k) = \sqrt{\frac{2S}{K}} \left(H(k)x(k)\alpha(0) + \sum_{n=0,\ n\neq k}^{K-1} H(n)x(n)\alpha(k-n) \right) + z(k), \tag{2}$$

where S is the average transmission power, K is the number of subcarriers, and $H(k)$, $x(k)$, $a(k)$, and $z(k)$ are the channel response, transmitted signal, CPE due to the PN, and $z(k)$ is additive white Gaussian noise (AWGN) of the kth subcarrier, respectively. Fig. II-1.4-1 shows the infuluence of PN. In the time domain, the phase fluctuation is given by $q_i = q_{i-1} + w$, where the phase of the ith symbol and w is the PN as shown in II-1.4-1(a). Then, in the frequency domain, ICI occurs as shown in II-1.4-1(b). As a result, the orthgonality of OFDM is destroyed. Therefore, the PN compensation is necessary, and we achieve it by

the time window averaging for CTFI as shown in Sect. II-1.4.3. The channel state is estimated by the pilot signal, and the received signal of Eq. (2) is detected by the equalization with the PN compensation. After the QPSK demodulation, the detected signal is decoded, and the binary signal is output.

II-1.4.3. Phase Noise Compensation with Time Window Averaging

Fig. II-1.4-2 shows the time window averaging by TFI and CTFI. The conventional TFI pilot signal consists of $\{x(k)\} = \{1, 0, 1, 0, \ldots, 1, 0, 1, 0\}$, and two channel impulse responses are output in the time domain at the transmitter as shown in Fig. II 1.4-2(i)(a). Then, L channel impulse responses are output in the two time windows at the receiver as shown in Fig. II 1.4-2(i)(b). Conversely, in CTFI, four channel impulse responses are output in the time domain as shown in Fig. II-2.4.2(ii)(a). In this case, the time domain received signal for the CTFI is obtained as shown in Fig. II-3.4.2(ii)(b) by

$$\begin{aligned} \hat{h}(t) &= \sqrt{\frac{2S}{K}} h(\tau) \sum_{k=0}^{K-1} x(k) \exp\left(j2\pi \frac{kt}{K}\right) + z(t) \\ &= \sqrt{\frac{2S}{K}} \sum_{l=0}^{L-1} \sum_{w=0}^{3} \frac{h_l \delta(\tau - \tau_l - wN_g)}{\sqrt{2}} + z(t), \end{aligned} \tag{3}$$

where $z(t)$ is AWGN with influence of PN, N_g is the GI length, and h_l and τ_l are the complex channel gain and the delay time of the lth path, respectively. In this study, we assume $N_g = N_c / 4$. As a result, CTFI increases the amount of time windows. Here, since AWGN and PN follow a Gaussian distribution, their influences are mitigated by the time window averaging. In CTFI, the time windows for $[0, N_g - 1]$, $[N_g, 2N_g - 1]$, $[2N_g, 3N_g - 1]$, and $[3N_g, 4N_g - 1]$ are averaged. After applying FFT, the channel response is estimated as $\hat{H}(k)$. Moreover, to estimate the influence of PN, $\hat{H}(k)$ is returned to the time domain signal as shown in Fig. II-4.4.2(ii)(b) from

$$\begin{aligned} \tilde{h}(t) &= \sqrt{\frac{2S}{K}} \sum_{k=0}^{K-1} \hat{H}(k) \exp\left(j2\pi \frac{kt}{K}\right) + \tilde{z}(t) \\ &= \sqrt{\frac{2S}{K}} \sum_{l=0}^{L-1} h_l \delta(\tau - \tau_l) + \tilde{z}(t), \end{aligned} \tag{4}$$

where $\tilde{z}(t)$ is AWGN with the PN for $\mathrm{E}[|\tilde{z}(t)|]^2 = \mathrm{E}[|z(t)/4|]^2$, and $E[\cdot]$ is an ensemble average operation. Moreover, the channel impulse response between $[0, N_g - 1]$ for Eq. (4) is assigned as

$$\bar{h}(t) = \sqrt{\frac{2S}{K}} \sum_{l=0}^{L-1} \sum_{w=0}^{3} \frac{h_l \delta(\tau - \tau_l - wN_g)}{\sqrt{2}} + \frac{\tilde{z}(t)}{\sqrt{2}}. \tag{5}$$

Observing Eqs. (3) and (5), since the influence of PN is mitigated by the time window averaging, the influence of PN is estimated by

$$\sigma_{pro}^2 = \left|\hat{h}(t) - \bar{h}(t)\right|^2 . \tag{6}$$

By using the estimated power of PN, the received signal is detected by the MMSE as

$$\tilde{x}(k) = \frac{\hat{H}^*(k)y(k)}{|\hat{H}(k)|^2 + \sigma_{pro}^2}. \tag{7}$$

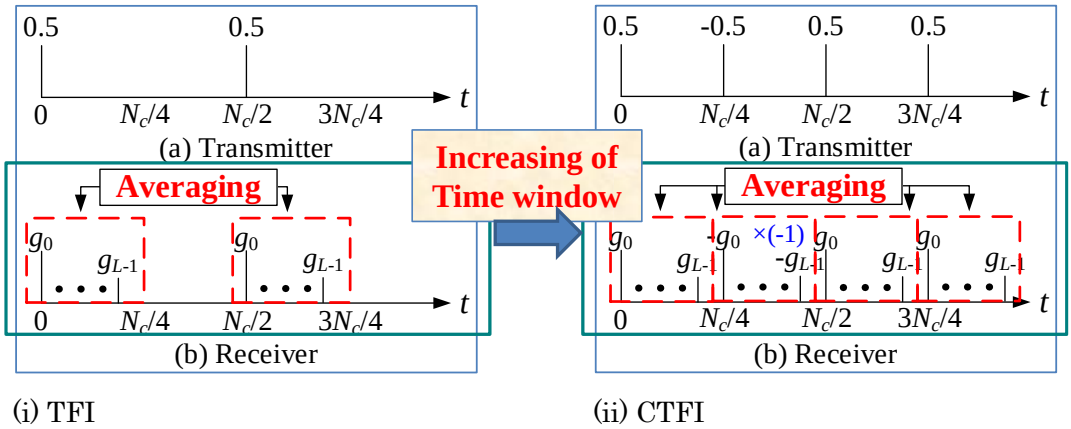

(i) TFI (ii) CTFI

Fig. II-1.4-2. Time window averaging by TFI and CTFI.

II-1.4.4. Computer Simulation Results

In this simulation, we assume CTFI-OFDM systems with $K = 64$ and $N_g = 16$. Then, coding rate and constraint length for forward error correction (FEC) are 1/2 and 7, the number of data and pilot symbols are 20 and 1, respectively, and modulation is quadrature-phase shift keying (QPSK). Moreover, the channel model is $L = 15$ path Rayleigh fading, and the OFDM symbol length is 10 μs. Fig. II-1.4-3 shows the bit error rate (BER) versus energy per bit to noise density ratio (E_b/N_0) for ZF and MMSE at the PN level of –80 dBc/Hz.

Observing Fig. II-1.4-3(a), the proposed CTFI-MMSE without FEC shows about 4 dB gain compared to the ZF at BER of 3×10^{-3}. Then, the proposed CTFI-ZF-FEC shows about 1.5 dB gain compared to the conventional TFI-ZF-FEC at BER of 3×10^{-4}. Moreover, the proposed CTFI-MMSE without FEC shows approximately the same BER performance as the conventional TFI-ZF-FEC. Also, the conventional TFI-ZF-FEC and CTFI-ZF-FEC without PN show approximately the same BER performance. However, the conventional TFI-ZF-FEC shows about 3 dB penalty due to PN. On the other hand, the proposed CTFI-ZF-FEC shows about 1 dB gain compared to the conventional TFI-ZF-FEC. Therefore, the time window averaging of CTFI is effective for the PN

compensation. Next, observing Fig. II-1.4-3(b), the conventional TFI-MMSE-FEC and propoposed CTFI-MMSE-FEC show the improved BER performance compared to the propoposed CTFI-MMSE without FEC. Then, the conventional CTFI-MMSE-FEC without PN shows about 0.5 and 3.5 dB gain compared to the conventional TFI-MMSE-FEC without and with PN at BER of 2×10^{-4}. On the other hand, the proposed CTFI-MMSE-FEC with PN shows about 1.5 dB gain compared to the conventional TFI-MMSE-FEC with PN. Therefore, the proposed method for CTFI and MMSE is also effective for the PN compensation.

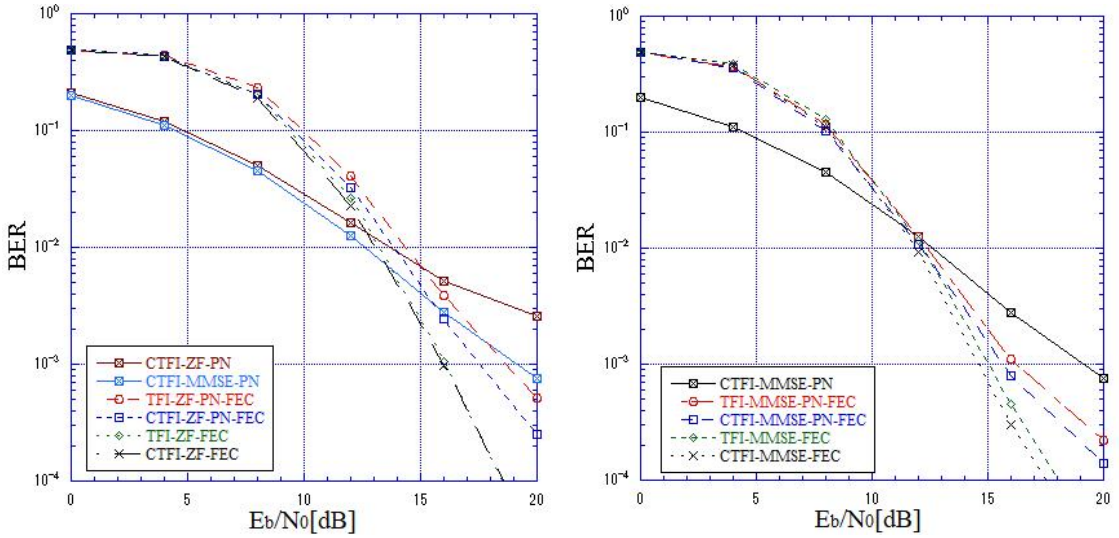

(a) ZF and MMSE w/ and w/o FEC (b) MMSE w/ FEC

Fig. II-1.4-3. BER vs. E_b/N_0 at –80 dBc/Hz.

II-1.4.5. Conclusion

In this study we have introduced the PN compensation with the time window averaging for CTFI-OFDM systems. In the proposed method, the influence of PN is mitigated by using the MMSE with the time window averaging for CTFI and WHT. From the computer simulation result, the proposed method has shown the improved BER performance and has obtained about 1.5 dB gain. Therefore, the proposed method for the time window averaging of CTFI is effective for PN compensation.

REFERENCE

[1] L. Zhang, A. Ijaz, P. Xiao, M. M. Molu, and R. Tafazolli, “Filtered OFDM systems, algorithms, and performance analysis for 5G and beyond,” IEEE Trans. on Commun., vol. 66, no. 3, pp. 1205–1218, March 2018.

[2] R. A. Casas, S. L. Biracree, and A. E. Youtz, “Time domain phase noise correction for OFDM signals,” IEEE Trans. on Broadcasting, vol. 48, no. 3, pp. 230–236, Sep. 2002.

[3] Q. Zou, A. Tarighat, and A. H. Sayed, “Compensation of phase noise in OFDM wireless systems,” IEEE Trans. on Signal Processing, vol. 55, no. 11, pp. 5407–5424, Nov. 2007.

[4] K. Zhi, C. Pan, H.~Ren, and K.~Wang, “Uplink achievable rate of intelligent reflecting surface-aided millimeter-wave communications with low-resolution ADC and phase noise,” IEEE Wirel. Commun. Lett., vol. 10, no. 3, pp. 654–658, March 2021.

[5] M. Renfors, I. P. Nasarre, T. Levanen, K. Pajukoski, and M. Valkama, “Phase noise resilient three-level continuous-phase modulation for DFT-spread OFDM,” IEEE Open J. of the Commun. Society, vol. 3, pp. 282–300, Feb. 2022.

[6] Y. Ida, C. Ahn, T. Matsumoto, and S. Matsufuji, “Four time windows averaging channel estimation with real and imaginary TFI pilot signals for OFDM,” IEICE Commun. Express, vol. 6, no. 10, pp. 590–595, Oct. 2017.

[7] S. Okamoto, Y. Ida, Y. Ohira, S. Kuroda, and T. Matsumoto, “Phase noise compensation with time window averaging for WHT-CTFI-OFDM,” 2024 IEEE 13th Global Conference on Consumer Electronics (GCCE2024), pp. 1392–1393, Oct. 2024.

II-1.5. Cooperative Positioning with User-Terminal Collaboration

Zhuoran Li and Osamu Muta
Kyushu University

Abstract—**This article describes a comprehensive analysis of RSS-based cooperative positioning schemes that use user-terminal collaboration over higher frequency bands, where an RSS-based cooperative user-positioning optimization problem is formulated and an iterative algorithm is derived to solve it. Using ray-tracing-based simulation in indoor environments, the effectiveness of the developed cooperative positioning algorithm was confirmed. Results obtained under various indoor conditions show that considerable performance improvement in user-positioning accuracy is obtained compared with results obtained using the traditional non-cooperative positioning scheme.**

II-1.5.1. Introduction

Accurate localization is increasingly recognized as a key enabler for next-generation wireless communication systems and location-aware services [1]. Several studies have been conducted to integrate sensing and communication functionalities [2]. However, traditional localization techniques, which typically rely on base station (BS)-user equipment (UE) link measurements, are often adversely affected by environmental factors such as multipath fading, non-line-of-sight (NLOS) conditions, and dynamic channel characteristics. The resultant inaccurate measurements can lead to marked positioning errors, especially in indoor environments, thereby limiting the performance of location-based applications.

User-terminal collaboration techniques, such as device-to-device (D2D) communication in the 5G standard, are emerging as a promising strategy for realizing spectrum-efficient and energy-efficient wireless communication systems. By enabling direct communications between nearby user terminals and by sharing their available resources such as antenna elements, marked improvements in system capacity and spectrum efficiency are expected. In earlier reports of the literature [3]-[5], downlink cooperative interference cancellation and related techniques have been proposed using direct communication between user terminals over a millimeter-wave frequency-band. They have been demonstrated to achieve a higher data rate than conventional non-cooperative methods. Using user-terminal collaboration is also an effective strategy for improving positioning accuracy toward advanced location-aware services. Cooperative localization techniques have been studied, such as those used for sensor networks and D2D-based mobile communication systems [6][7]. However, the achievable performance

improvement of cooperative positioning with high-frequency-band collaboration has not been clarified sufficiently.

This article presents a comprehensive evaluation of RSS-based cooperative positioning schemes that use user-terminal collaboration over higher frequency bands, subsequently clarifying the achievable positioning accuracy in various indoor scenarios [8][9]. After formulating an RSS-based cooperative positioning optimization problem, we derive an iterative algorithm to solve it. Simulation results obtained under various conditions demonstrate that the developed cooperative algorithm achieves marked performance improvement compared to the traditional non-cooperative algorithm.

II-1.5.2. System Model and Technical Details

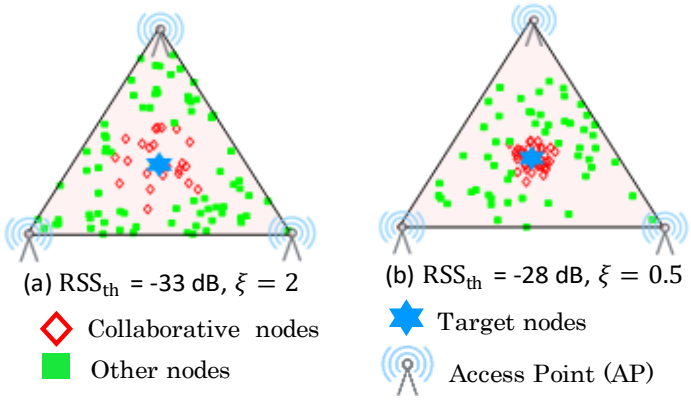

Fig. II-1.5-1 Simulation setup [8].

The system comprises multiple BSs and UEs, each equipped with two wireless interfaces: one for sub-6 GHz BS-to-UE (B2U) links and one for higher-frequency-based inter-UE collaboration. Figure II-1.5-1 portrays the simulation setup, where a particular target node is represented by a blue hexagon, its collaborative nodes are denoted by red diamonds, where the green square terminals with low RSS are unable to collaborate with the target node. All terminals in the service area receive signals from BSs. All information can be shared among BSs, which have fixed and known locations. Terminals can establish cooperative links when the received signal strength between these terminals exceeds a threshold. Consequently, each terminal estimates its own position based on the information obtained from the connected AP and the cooperating terminals. The difference of user distribution between Figs. II-1.5-1(a) and II-1.5-1(b) is governed by $f(d) = \frac{\xi\, d^{\xi-1}}{C\, R^{\xi}}$, where C is a normalization constant. Also d represents the distance from the UE to the geometric center of the cell. More specifically, $\xi = 2$ gives a uniform distribution: a value of ξ close to zero gives a concentrated user distribution as the figure shows.

The deterministic path loss model is given as $PL(d) = 20\log_{10}\left(\frac{4\pi f_c}{c}\right) + 10\alpha\log_{10}(d)$ for $d > 1$ m. Therein, f_c stands for the carrier frequency, c represents the speed of light, and α stands for the path loss exponent. The estimated distance is then given as $\hat{d}_{i,j} = 10^{-\frac{Z_{i,j}(\alpha)}{10\alpha}}$, where $Z_{i,j}(\alpha)$ is the RSS at node i from node j.

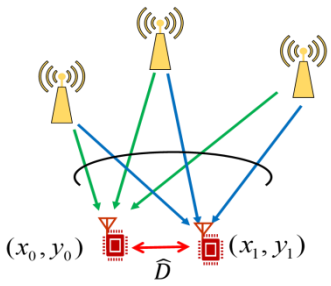

Fig. II-1.5-2 Principle of cooperative positioning.

II-1.5.3. Localization Methodology

II-1.5.3.1. Baseline Non-Cooperative Positioning

Each UE estimates its position based on RSS measurements from BSs. Letting the unknown position of UE i be $\mathbf{p}_i = [x_i, y_i]^{\mathrm{T}}$ and letting S_i denote the set of BSs with known positions $\mathbf{p}_j$, then the squared Euclidean distance is $\|\mathbf{p}_i - \mathbf{p}_j\|^2 = \|\mathbf{p}_i\|^2 - 2\mathbf{p}_j^{\mathrm{T}}\mathbf{p}_i + \|\mathbf{p}_j\|^2$. Equating this to the squared measured distance $\hat{d}_{i,j}^2$ yields $\|\mathbf{p}_i\|^2 - 2\mathbf{p}_j^{\mathrm{T}}\mathbf{p}_i = \hat{d}_{i,j}^2 - \|\mathbf{p}_j\|^2$. Defining $\boldsymbol{\theta}_i = [x_i, y_i, \|\mathbf{p}_i\|^2]^{\mathrm{T}}$, then, for each $j \in S_i$, the equation above can be written as $\mathbf{a}_j\boldsymbol{\theta}_i = b_j$, where $\mathbf{a}_j = [-2x_j \quad -2y_j \quad 1], b_j = \hat{d}_{i,j}^2 - \|\mathbf{p}_j\|^2$. The least-squares solution is then obtained by stacking the above equations, from which the estimated position $\hat{\mathbf{p}}_i$ is extracted.

II-1.5.3.2. Cooperative Localization with User Collaboration

To improve the localization accuracy further, UEs share their RSS measurements with neighboring UEs, thereby extending the effective set S_i to include both BSs and UEs. As presented in Fig. II-1.5-2, the red arrow represents the collaboration link, from which distance estimation $\widehat{D}$ is made. The core idea is to manipulate the estimated position from AP signals such that the final result has the smallest sum-of-square error compared to the distance estimation from the collaboration link. Therefore, the cooperative problem is formulated as minimizing the cost function as shown below.

$$C(\mathbf{r}) = \sum_{i=1}^{M}\sum_{j\in S_i} w_j \left(\hat{d}_{i,j} - \|\mathbf{p}_i - \mathbf{p}_j\|\right)^2 \tag{1.5-1}$$

Therein, w_j are weight factors emphasizing reliable measurements. Also, $\mathbf{r}$ denotes the collection of all UE positions. An iterative steepest descent method is used to update the position estimates as

$$\mathbf{p}_i^{(l)} = \mathbf{p}_i^{(l-1)} + \delta_i^{(l)} \sum_{j \in S_i} w_j \left(\hat{d}_{i,j} - \left\| \mathbf{p}_i^{(l-1)} - \mathbf{p}_j^{(l-1)} \right\| \right) \frac{\mathbf{p}_i^{(l-1)} - \mathbf{p}_j^{(l-1)}}{\left\| \mathbf{p}_i^{(l-1)} - \mathbf{p}_j^{(l-1)} \right\|}, \quad (1.5\text{-}2)$$

with $\delta_i^{(l)}$ as the step size at iteration l.

II-1.5.4. Performance Evaluation

II-1.5.4.1. Simulation Setup

To evaluate the effectiveness of the user-terminal cooperation-based positioning algorithm, a ray tracing-based simulation is performed. For the statistical model, the simulation assumes a Rician fading environment, with 3 BSs and 50 UEs in the target area. The distance of each BS is 200 m; UEs are distributed inside the triangle that BSs form. Also, OFDM transmission with 64 subcarriers is assumed. The Rician factors are set as 7 dB and 15 dB, respectively, for BS-to-UE and inter-UE connections. The UEs are assumed to be static. The transmission power of BSs is set as 30 dBm, whereas the collaboration link power is set as 20 dBm. The noise power spectral density is set as -174 dBm/Hz. The simulation varied the collaboration link RSS detection threshold from -36 dB to -33 dB, and varied the user concentration parameter ξ from 0 to 2.

For ray-tracing method, when a 33×38 m^2 indoor environment is considered, 4 APs are placed. Also, 10 UEs are distributed uniformly in a square region. The maximum number of reflections in the environment is set as 3. The number of collaborating UEs is 10. The center frequencies of APs and UEs are set respectively as 5.18 GHz and 28 GHz. The users are assumed to be static. The walls are considered to be wooden, whereas the ceiling and floor are considered to be concrete during the ray tracing simulation. The simulation varied the number of observed RSS values for averaging from 1 to 8. The APs are either positioned at the corners of the room, or next to the distributed user area.

II-1.5.4.2. Simulation Results and Discussion

Figure II-1.5-3 presents an illustration of the effects of concentration parameter ξ and connection RSS threshold on the positioning error. The result is acquired using the statistical model. Specifically, we vary ξ from a value close to 0 (highly concentrated user distribution) to $\xi = 2$ (uniform distribution). Figure II-1.5-3 presents the cumulative distribution function (CDF) of the positioning error for different values of ξ. The results demonstrate that a more concentrated distribution (lower ξ) tends to yield a higher number of cooperative links, thereby reducing positioning errors. Additionally, the lower RSS allowance is observed to lead to a better positioning result because of better connectivity.

The effect of increasing the number of averaged RSS measurements (denoted as N_A) on the positioning accuracy is shown in Fig. II-1.5-4: a ray-trace-based simulation scenario. Its results are shown where UEs are distributed uniformly throughout the service area. It is apparent from this figure that increasing N_A reduces the positioning error consistently, demonstrating the benefit of averaging in mitigating random fluctuations attributable to the multipath effect.

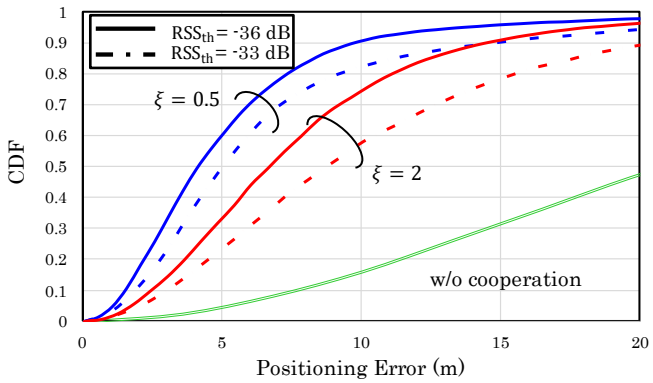

Fig. II-1.5-3 CDF of positioning errors for different values of concentration parameter ξ [8].

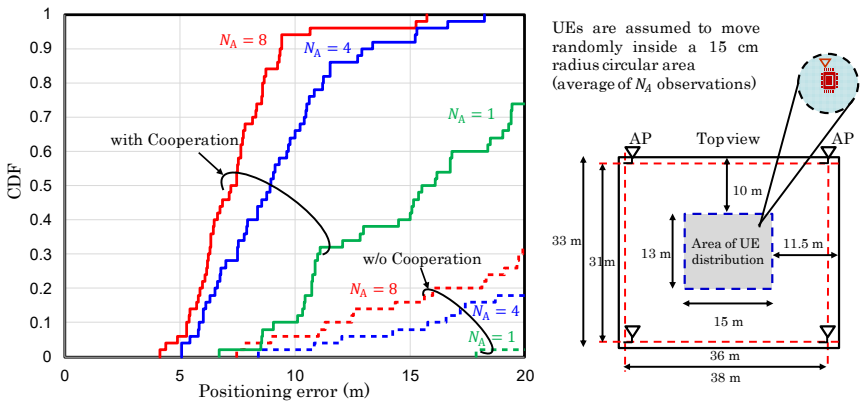

Fig. II-1.5-4 CDF of positioning errors in a uniform indoor environment with different numbers of averaged RSS measurements (N_A) [9].

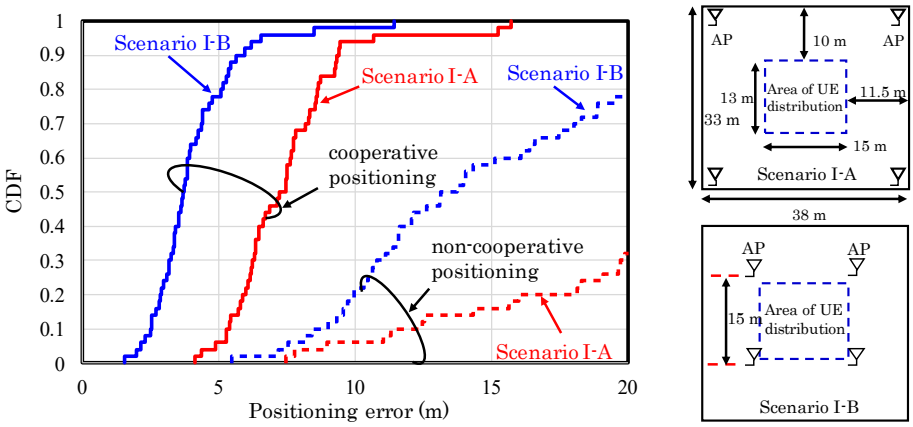

Fig. II-1.5-5 Effects of increased direct wave strength on positioning accuracy [9].

In Fig. II-1.5-5, to analyze the effect of the direct wave component, we perform simulations in which the BSs are placed closer to the UEs, thereby increasing the strength of the direct line-of-sight (LOS) component relative to the multipath reflections. The result is captured using a ray-tracing model. The UE positions remain unchanged. Only the BS positions are adjusted. Figure II-1.5-5 depicts that the positioning accuracy improves considerably when the direct wave is dominant, even under difficult multipath conditions. This result emphasizes the importance of BS placement and its influence on cooperative positioning performance.

II-1.5.5. Conclusion

This report has described evaluation of the achieved performance of RSS-based cooperative positioning. The simulation results demonstrated that the proposed approach mitigates the influence of multipath fading effectively and provides considerable improvements in positioning accuracy for indoor environments. The effects associated with various scenarios such as RSS threshold for cooperation, user distribution, and direct wave component strength were also investigated.

REFERENCES

[1] NTT Docomo, White Paper 5G Evolution and 6G (ver. 5.0), https://www.docomo.ne.jp/english/corporate/technology/whitepaper_6g/.

[2] Y. Cui, F. Liu, X. Jing, and J. Mu, "Integrating sensing and communications for ubiquitous IOT: applications, trends, and challenges," IEEE Network, vol. 35, no. 5, pp. 158-167, Sep. 2021.

[3] H. Murata and R. Shinohara, "Performance improvement of ZF-precoded MU-MIMO transmission by collaborative interference cancellation," IEICE Communications Express, vol. 5, pp. 155-160, 2015.

[4] H. Taromaru, H. Murata, T. Nakahira, D. Murayama, and T. Moriyama, “Error control on mobile station sides in collaborative multiple-input multiple-output systems,” IEEE Access, vol. 10, pp. 26493-26500, 2022.

[5] F. Du, H. Murata, M. Kasai, T. Nakahira, K. Ishihara, M. Sasaki, and T. Moriyama, “Distributed detection of MIMO Spatial Multiplexed Signals in Terminal collaborated reception,” IEICE Trans. Commun., vol. E104.B, no. 7, pp. 884–892, Jul. 2021.

[6] H. Wymeersch, J. Lien, and M. Z. Win, “Cooperative localization in wireless networks,” Proceedings of the IEEE, vol. 97, no. 2, pp. 427–450, Feb. 2009.

[7] M. Ammous, H. Chen, H. Wymeersch, and S. Valaee, “3D cooperative positioning via RIS and Sidelink communications with Zero access points,” IEEE Trans. Mob. Comput., pp. 1–18, Feb. 2025.

[8] Z. Li, O. Muta and Y. Jitsumatsu, “Performance Evaluation of Cooperative Positioning with User-Terminal Collaboration,” International Japan–Africa Conference on Electronics, Communications and Computations (JAC-ECC), pp. 240-243, Dec. 2023.

[9] Z. Li, O. Muta and Y. Jitsumatsu, “Performance of RSS-Based Indoor Cooperative Positioning with Weighted User-Terminal Collaboration,” International Japan–Africa Conference on Electronics, Communications and Computations (JAC-ECC), Dec. 2024.

II-1.6. Access Control for Terminal Collaborative Communication System

Hiraku Okada, Yiche Li
Nagoya University

Abstract— In a terminal collaborative wireless communication system, neighboring terminals collaborate by sharing transmission information. They form a virtual, large-scale multi-input multi-output (MIMO) system to achieve spatial multiplexing. This study leverages millimeter-wave communication, which is known for high speed and low latency, to facilitate information sharing between terminals. The main goal of our study is to evaluate the performance of inter-terminal access control in a millimeter-wave-based collaborative system. To enhance the efficiency of virtual MIMO, information must be broadly shared among terminals. This research investigates how access control affects the number of coordinating terminals under millimeter-wave communication. Our findings indicate that access control significantly mitigates interference and increases the coordination between terminals. Additionally, it is evident that the effectiveness of coordination is highly influenced by the radio wave propagation environment.

II-1.6.1. Introduction

The ubiquity of wireless communication devices, particularly smartphones, has led to greatly increased communication traffic. This surge has intensified the demand for frequency resources, which are limited [1]. Consequently, the congestion and interference that affect these resources degrade the quality and efficiency of communication. Addressing the efficient allocation of frequency resources and improving the quality of communication are critical challenges in wireless technology. In the context of Beyond 5G/6G, innovative technical solutions are essential to robust, high-speed data transmission. This study focuses on millimeter-wave-based collaborative communication for terminals as a strategic solution [2]. This approach optimizes frequency resource utilization by enabling devices to collaborate and form a virtual large-scale multi-input multi-output (MIMO) system.

Unlike conventional systems where base stations (BSs) communicate directly with terminals, this collaborative model establishes a large virtual terminal through multi-terminal collaboration, where the capacity of the communication channel scales with the number of antennas [3][4]. This optimizes the usage of traditional frequency bands and necessitates that terminals share data via millimeter-wave communication, which provides ample resources and supports rapid, low-latency transmission [5].

This study aims to evaluate the performance of inter-terminal access control in a collaborative system for terminals that are based on millimeter-wave wireless

communications. To enhance the efficiency of the virtual MIMO system enabled by terminal collaboration, the transmitted information must be shared with a large number of terminals. Therefore, this study investigates how the number of collaborating terminals varies when simple access control is used in a model designed for millimeter-wave communication.

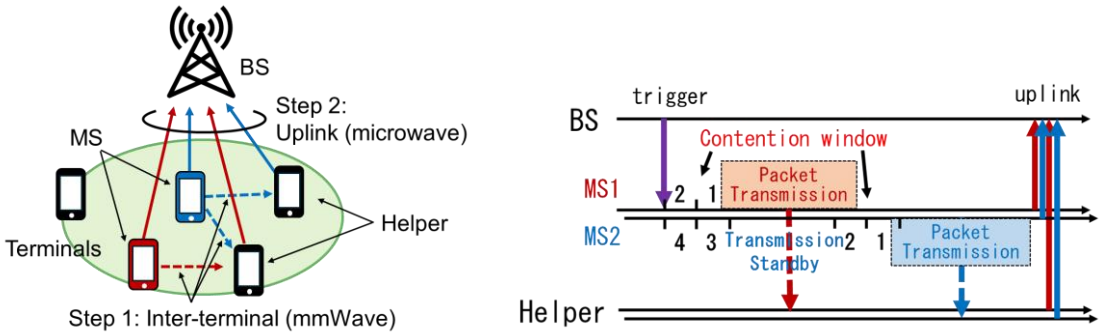

(a) System model. (b) Timing chart of access control.

Fig. II-1.6-1. System model and access control [6].

II-1.6.2. System Model

Figgure II-1.6-1(a) presents the system model assumed in this study. The system consists of a BS and a group of terminals. We first consider the uplink from the terminals to the BS. The terminal collaborative communication system involves inter-terminal communication, where terminals share information among themselves, and uplink communication, where multiple terminals collaborate to transmit to the BS. Millimeter waves, which offer high-speed, large-capacity, and low-latency transmission, are used for inter-terminal communication, whereas microwaves are used for uplink communication to enable long-distance transmission. This study focuses on inter-terminal communication.

As illustrated in Fig. II-1.6-8(a), the terminal group includes the mobile station (MS), Helpers (collaborative terminals), and other terminals. The MS is essential, as it holds information that is destined for the BS and broadcasts this information to other terminals through the inter-terminal communication channels to facilitate information sharing. This process converts the receiving terminals to collaborative Helpers for effective uplink transmission.

Helpers have the ability to receive information from multiple MSs. Considering this, two uplink transmission methods are evaluated: the single transmission method, which selects the information with the highest received power from among the MSs for the uplink, and the superposition transmission method, which leverages the multiple

antennas of the Helpers to amalgamate and more efficiently transmit the information received from various MSs.

II-1.6.3. Access Control

In this section, we discuss access to the inter-terminal communication channel, where the BS initiates the interaction by sending a trigger signal. When a MS receives this signal, it broadcasts its information. Without access control, the simultaneous transmissions from multiple MSs would degrade the SINR, which could result in failures of reception and insufficient Helper numbers. To address this, we introduce and evaluate a simple access control mechanism, which is depicted in Fig. II-1.6-1(b).

This study implements access control based on the IEEE 802.11 Distributed Coordination Function (DCF). The DCF protocol manages interference and prevents collisions using a contention window and the carrier sensing by each MS. Before transmitting a signal, each MS randomly selects a number, CW, from the contention window range, and it aligns its transmission to the timing slots while performing carrier sensing. If a channel is busy, the MS delays its transmission to prevent a collision. Fig. II-1.6-(b) shows two MSs, MS1, and MS2, selecting different CW values and checking if the channel is busy. MS1 transmits first; MS2, detecting that the channel is busy, postpones its transmission, thereby facilitating time division rather than simultaneous transmissions, which helps prevent potential collisions.

II-1.6.4. Numerical Results

In this study, the 3GPP 28 GHz band millimeter-wave indoor communication model is used as the radio propagation model for the inter-terminal communication channels [7]. This model provides a definition for two types of environments: the Open-Office environment, which is relatively open, and the Mixed-Office environment, which contains obstacles. The target area is 120 m × 50 m. The simulations varied the number of MSs from 1 to 10, for a total of 200 terminals. Access control utilized a contention window from 0 to 31, with a fixed transmission power of 23 dBm. Signal quality was assessed by setting the standard deviation of shadowing σ_{SF} to 3 dB under line-of-sight (LOS) conditions and to 8.03 dB under non-LOS (NLOS) conditions. The system's noise figure was 9 dB, the room temperature was 300 K, the carrier sense threshold was set at -82 dBm, and the SINR threshold was set to 10 dB. Under these conditions, terminals transmitted packets according to access control. Each terminal calculated its own SINR, and successful communication was defined as exceeding the threshold. To ensure data reliability, 500 trials were conducted.

Figure II-1.6-2 shows the number of Helpers per MS in Open-Office and Mixed-Office environments. Without access control, the number of collaborative terminals decreases sharply as the number of MSs increases. Access control mitigates this decrease by reducing interference, which is particularly effective for superposition transmissions. When the access control is not used, the Open-Office environment has more Helpers when the number of MS is small, but the Mixed-Office environment has more Helpers when the number of MS is large. This is because the Mixed-Office environment has a higher probability of NLOS, resulting in less interference. When access control is used, the number of Helpers in a Mixed-Office environment is lower than in an Open-Office environment. This is due to the higher probability of NLOS conditions and the significant impact of hidden terminals. The higher incidence of hidden terminals reduces the number of effective Helpers in the Mixed-Office environment.

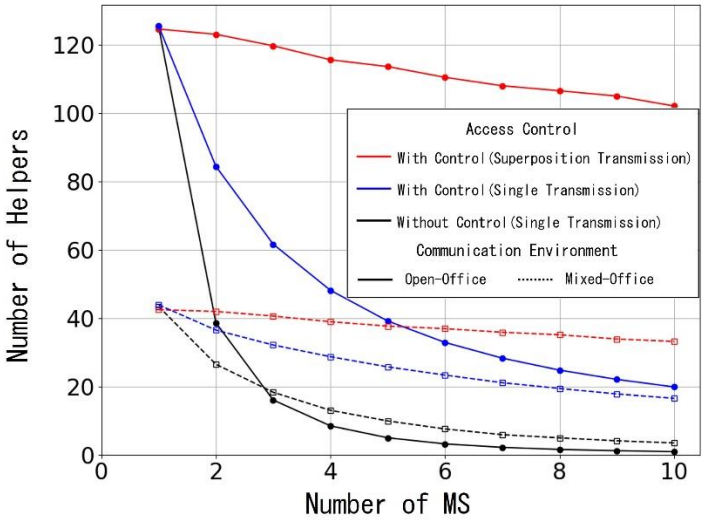

Fig. II-1.6-2. Number of helpers per MS [6].

II-1.6.5. Conclusion

In this study, we investigated how the number of collaborative terminals in a millimeter-wave-based terminal collaborative communication system is affected by the imposition of access control. The results showed that access control effectively reduces interference between MSs, which leads to an increase in the number of collaborative terminals. Additionally, the number of collaborative terminals greatly depends on the radio propagation environment. It was observed that the effects of access control and the impact of hidden terminals vary between Open-Office and Mixed-Office environments, and this results in different numbers of collaborative terminals.

REFERENCE

[1] ITU-R, “IMTVision - Framework and overall objectives of the future development of IMT for 2020 and beyond,” M.2083, 2023.

[2] H. Murata, Y. Ida, K. Maruta, Y. Jitsumatsu, O. Muta, H. Okada, E. Okamoto, Y. Sanada, T. Nishimura, and S. Denno, “[Invited Lecture] Novel wireless communication system realized by mobile terminal collaboration - Recent results and application to uplink transmission -,” IEICE Technical Report, RCS2022-149, pp.107–107, Oct. 2022.

[3] A. Saad, M. Ismail, and N. Misran, “Capacity of MIMO channels at different antenna configurations,” J. Appl. Sci., vol.8, pp.4595–4602, 2008.

[4] R.W. Heath, N. Gonz´alez-Prelcic, S. Rangan, W. Roh, and A.M. Sayeed, “An overview of signal processing techniques for millimeter wave MIMO systems,” IEEE J. Sel. Top. Signal Process., vol.10, no.3, pp.436–453, April 2016.

[5] A. Ghosh, A. Maeder, M. Baker, and D. Chandramouli, “5G evolution: A view on 5G cellular technology beyond 3GPP release 15,” IEEE Access, vol.7, pp.127639–127651, 2019.

[6] Y. Li, H. Okada, and C. Ben Naila, “Evaluation of access control mechanisms within inter-terminal cooperation in millimeter-wave communication systems,” IEICE International Conference on Emerging Technologies for Communications (ICETC), P1-04, 2024.

[7] 3GPP, “Study on channel model for frequencies from 0.5 to 100 GHz,” TR. 38.901, v16.1.0, Jan. 2020.

II-1.7. Terminal Grouping Based on Instantaneous Throughput

Yukitoshi Sanada and Eiku Ando
Keio University

Abstract—This research proposes a grouping scheme that takes instantaneous throughput into account is proposed for collaborative MIMO reception and its performance is evaluated. As for the grouping scheme in the collaborative MIMO reception, either the number of user equipments (UEs) in each group or user fairness have been included in previous research. However, correlation among UE antennas deteriorates performance. Thus, this section proposes a grouping scheme that selects the subgroup of UEs within each group based on an instantaneous throughput and a fairness index among UEs. The criterion in the proposed scheme decreases correlation among UE antennas in each group and realizes less degradation of the user throughput compared to those with the conventional scheme. Numerical results obtained through computer simulation show that the proposed scheme has achieved about 1.1 times higher user throughput compared to the conventional scheme.

II-1.7.1. Introduction

Terminal collaborative MIMO reception is expected to be utilized in the fifth generation (5G) mobile communication and beyond as an effective way to maximize the use of the Sub-6 GHz band [1]. In terminal collaborative MIMO reception, a larger number of terminals in a group increases the number of MIMO signal streams, which is expected to improve system throughput. Therefore, a grouping scheme in conventional research has taken communication range in the millimeter-wave band into account and has tried to form groups locally while maximizing the number of terminals within each group [2]. However, when the correlation between antennas in the Sub-6 GHz band is high, the throughput decreases. To address this issue, this research investigates a grouping scheme that is based on instantaneous throughput in the Sub-6 GHz band.

II-1.7.2. System Model

The base station is assumed to be equipped with a full-digital massive MIMO antenna and realize beamforming on the downlink for each terminal. After beamforming, the channel response matrix on the kth subcarrier of the gth group is given by

$$\mathbf{H}^{g}[k] = \left[\mathbf{H}^{g}_{1,1}[k] \quad \cdots \quad \mathbf{H}^{g}_{N_x,N_z}[k]\right] \quad , \tag{1}$$

where the channel responses for the (n_x, n_z)th antenna element of the massive MIMO antenna is

$$\mathbf{H}^{g}_{1,1}[k] = \left[H^{g1}_{n_x,n_z}[k] \quad \cdots \quad H^{gN^{g}_{R}}_{n_x,n_z}[k]\right]^{\mathrm{T}} \quad , \tag{2}$$

where N_R^g is the number of UEs in the gth group and $\mathbf{A}^{\mathrm{T}}$ represents the transpose matrix of $\mathbf{A}$. The beamforming weight matrix $\mathbf{W}^g[k]$ is given as

$$\mathbf{W}^g[k] = \left[\mathbf{W}_{n_x,n_z}^{l_g m_g g1}[k] \quad \dots \quad \mathbf{W}_{n_x,n_z}^{l_g m_g gj}[k] \quad \dots \quad \mathbf{W}_{n_x,n_z}^{l_g m_g N_R^g}[k]\right] \quad , \tag{3}$$

where $\mathbf{W}_{n_x,n_z}^{l_g m_g gj}[k]$ is the beamforming weight vector for the jth receive antenna is given as

$$\mathbf{W}_{n_x,n_z}^{l_g m_g gj}[k] = \left[\mathbf{W}_{1,1}^{l_g m_g gj}[k] \quad \dots \quad \mathbf{W}_{N_x,N_z}^{l_g m_g gj}[k]\right] \quad , \tag{4}$$

The signals of UEs for each group are demodulated jointly with linear minimum mean square error (MMSE) detection. The signal-to-interference-and-noise (SINR) of the jth receive antenna in the gth group is given as

$$SINR_j[k] = \frac{\beta_j^g[k]}{1-\beta_j^g[k]} \quad , \tag{5}$$

where

$$\beta_j^g[k] = \left(\mathbf{H}^g[k]\mathbf{W}^g[k](\mathbf{H}^g[k]\mathbf{W}^g[k])^{\mathrm{H}} + \frac{N_T\sigma_n^2}{P_t}\mathbf{I}_{N_R^g}\right)^{-1}(\mathbf{H}^g[k]\mathbf{W}^g[k])_j \quad , \tag{6}$$

where $\mathbf{I}_{N_R^g}$ is $N_R^g \times N_R^g$ identity matrix and $\mathbf{A}^{\mathrm{H}}$ denotes the Hermitian transpose of a matrix $\mathbf{A}$, P_t is the transmission power, N_T is the number of antenna elements of the massive MIMO, and σ_n^2 is the noise variance. Furthermore, $(\mathbf{A})_j$ means the jth column of a matrix $\mathbf{A}$. Thus, the throughput of the uth UE with the rth resource block assigned to the UE in the tth timeslot is represented as

$$T_u^g(t,r) = \sum_{k=12r-11}^{12r}\sum_{j\in Q_u^g}\log_2\left(1+SINR_j[k]\right) \quad , \tag{7}$$

where Q_u^g is the set of indexes of the receive antennas equipped with the uth UE in the gth group.

II-1.7.3. Grouping Scheme

II-1.7.3.1. Conventional Grouping Scheme

An example of the conventional grouping scheme is shown in Fig. II-1.7-1. In the conventional grouping scheme, a UE forms a pseudo group with UEs that can communicate with a signal-to-noise ratio (SNR) of more than a threshold ω. In this example, UE3 can communicate with UE1, UE2, and UE4. However, the signal from UE4 reaches UE1 or UE2 with the power of less than ω. Thus, UE4 is excluded from the group. Furthermore, the SNR range of the received signals in the Sub-6 band is limited to improve the fairness of

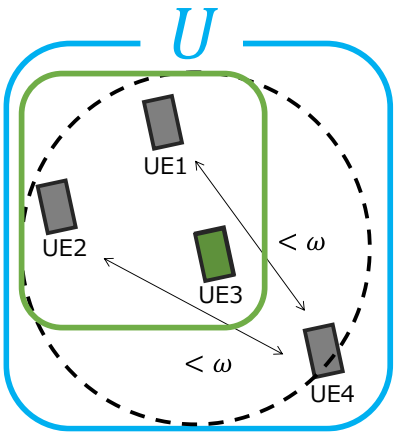

Fig. II-1.7-1.
Conventional grouping scheme.

the UEs in the pseudo group and UEs whose signal SNR is out of this range are excluded from the pseudo group. The pseudo group with the largest number of UEs in the group is adopted as a group and the other UEs try to form a new group. Each UE may form a group with only one terminal. This process is repeated until all the UEs belong to the group.

II-1.7.3.2. Proposed Grouping Scheme

An example of the proposed grouping scheme is shown in Fig. II-1.7-2. In the proposed grouping scheme, UEs in each group formed by the conventional grouping scheme are divided into subgroups as shown in Fig. II-1.7-3. The instantaneous throughputs of UEs in those subgroups are calculated and each set of subgroups are evaluated through an evaluation function.

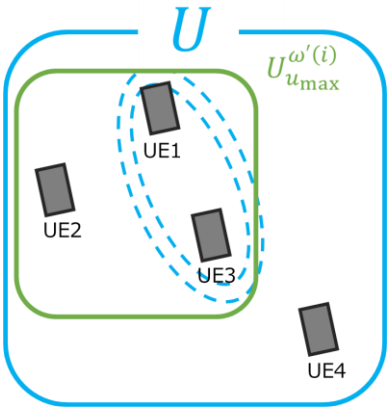

Fig. II-1.7-2.
Proposed grouping scheme.

Suppose that N_{RB} is the number of resource blocks, the instantaneous throughput of the uth UE that belongs to the mth subgroup of the ith group is calculated as

$$T_u^{i(m)}(t) = \sum_{r=1}^{N_{RB}} T_u^{i(m)}(t,r) \quad , \qquad (8)$$

where $T_u^{i(m)}(t,r)$ is the uth UE that belongs to the mth subgroup of the ith group on the rth resource block and it is calculated from Eq. (7). The instantaneous fairness is calculated as follows;

$$F_u^{i(m)}(t) = \frac{\left(\sum_{u \in U_{u_{max}}^{\omega'(i)}} T_u^{i(m)}(t)\right)^2}{\left|U_{u_{max}}^{\omega'(i)}\right|^2 \sum_{u \in U_{u_{max}}^{\omega'(i)}} T_u^{i(m)}(t)^2}, \qquad (9)$$

Index m	Subgroup	Th	FI
1	(UE1, UE2, UE3)	$\sum T_u^{i(1)}(t)$	$F_{\text{ins}}^{i(1)}$
2	(UE1, UE2), UE3	$\sum T_u^{i(2)}(t)$	$F_{\text{ins}}^{i(2)}$
3	(UE2, UE3), UE1	$\sum T_u^{i(3)}(t)$	$F_{\text{ins}}^{i(3)}$
4	(UE3, UE1), UE2	$\sum T_u^{i(4)}(t)$	$F_{\text{ins}}^{i(4)}$
5	UE1, UE2, UE3	$\sum T_u^{i(5)}(t)$	$F_{\text{ins}}^{i(5)}$

Fig. II-1.7-3. Subgrouping of proposed grouping scheme.

where $U_{u_{max}}^{\omega'(i)}$ is the set of UE indexes that belongs to ith group. Based on Eqs. (8) and (9), the following evaluation function is defined.

$$J\left(T_u^{i(m)}(t), F_u^{i(m)}(t) | u \in U_{u_{max}}^{\omega'(i)},\right) = \gamma \sum_{u \in U_{u_{max}}^{\omega'(i)}} T_u^{i(m)}(t) + (1-\gamma) F_u^{i(m)}(t), \qquad (10)$$

where γ is the trade-off weight between the group throughput and the fairness index.

II-1.7.4. Performance Evaluation

II-1.7.4.1. Simulation Conditions

The performance of the conventional and proposed grouping schemes are obtained through computer simulation. The center frequencies of the Sub-6 band and the

millimeter wave band are 5.2 GHz and 28 GHz, respectively. The bandwidths for the Sub-6 band and the millimeter wave band are 34.56 MHz and 40 MHz. The number of subcarriers is 288, the number of time slots is 100, and the number of symbols in each time slot is 7. The massive MIMO base station transmits signals using 128 antenna elements, comprising 16 horizontal and 8 vertical elements. The antenna spacing is 2.88 cm. The total transmit power of the base station is 30 dBW and each antenna element transmits 1000/128 mW. The UE transmit power is 20 dBm. The number of UEs in a cell is 12 and each UE has one antenna element. The cell radius is 250 meters and UEs are randomly positioned within the cell. The SNR threshold in the millimeter band is set to 10dB. In the conventional scheme, the SNR range of the received signal in the Sub-6 band is 5, 10, or 30dB. A CDL-A channel model is assumed for line-of-sight (LOS) conditions and a CDL-D channel model is assumed for non-line-of-sight (NLOS) conditions [3]. The pass loss exponent of LOS conditions is 2.1 dB and that of NLOS conditions is 3.53 dB in the Sub-6 band. The pass loss exponent of LOS conditions is 2 dB and that of NLOS conditions is 3.2 dB in the millimeter wave band [4]. The shadow fading standard deviation of LOS conditions is 4 and that of NLOS conditions is 7.82 in the Sub-6 band. The shadow fading standard deviation of LOS conditions is 4 and that of NLOS conditions is 7 in the millimeter band. The trade-off weight of the proposed scheme is 1, 0.001, or 0. The noise spectrum density is -174 dBm/Hz and the noise figure is set to 9 dB.

II-1.7.4.2. Numerical Results

The cumulative distribution function (CDF) of channel correlation among UEs are shown in Fig. II-1.7-4. The channel correlation with the conventional grouping scheme is relatively higher regardless of the SNR range values. This is because the UEs that are positioned closely tend to have the same sort of signal levels. On the other hand, the proposed grouping scheme tries to increase the instantaneous throughput, especially when the trade-off weight γ is set to 1. When the trade-off weight γ is set to 0, the fairness among UEs is improved so that the UEs that are positioned closely tend to form a group.

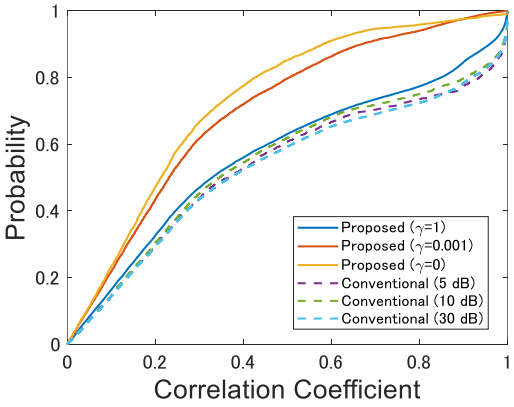

Fig. II-1.7-4. CDF of channel correlation.

The relationship between the throughput and the fairness index is shown in Fig. II-1.7-5. The throughput improves for a trade-off weight of 1 and the fairness index improves for a trade-off weight of 0. For a fairness index of 0.87, the throughput with the proposed grouping scheme improves by a factor of 1.13 as compared to that with the conventional grouping scheme.

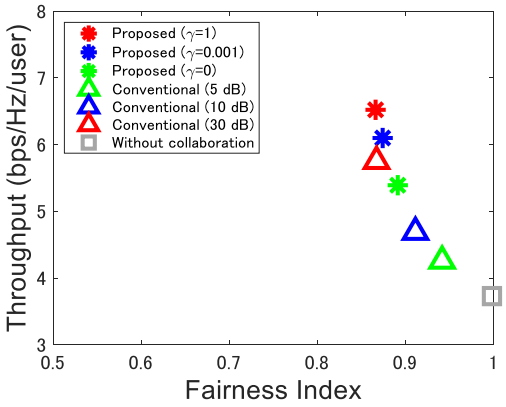

Fig. II-1.7-5. Throughput vs. fairness.

II-1.7.5. Conclusions

In this research a grouping scheme that selects the subgroup of UEs within each group based on an instantaneous throughput and a fairness index among UEs is proposed. The criterion in the proposed grouping scheme decreases correlation among UE channels in each group and realizes less degradation of the user throughput compared to those with the conventional scheme. Numerical results obtained through computer simulation show that the proposed scheme has achieved about 1.1 times higher user throughput compared to the conventional scheme.

REFERENCE

[1] Y. Hayashi, I. Shubhi, and H. Murata, "User Collaboration for Interference Cancellation on Multi-User MIMO Communication Systems," IEEE 82nd Vehicular Technology Conference, Sept. 2015.

[2] E. Ando and Y. Sanada, "Performance of Collaborative MIMO Reception with User Grouping Schemes," IEICE Trans. on Commun., vol. E107-B, no. 1, Jan. 2024.

[3] "Study on Channel Model for Frequencies from 0.5 to 100 GHz," 3GPP TR 38.901, vol. 17.0.0, Apr. 2020.

[4] T. S. Rappaport, G. R. MacCartney, M. K. Samimi, and S. Sun, "Wideband Millimeter-Wave Propagation Measurements and Channel Models for Future Wireless Communication System Design (Invited Paper)," IEEE Transactions on Communications, vol. 63, no. 9, Sept. 2015.

II-1.8. Impact of Signaling Overhead in Uplink Collaborative MIMO Transmission

Kazuki Maruta and Anbo Yue
Tokyo University of Science

***Abstract*— Terminal-collaborative Multiple-Input Multiple-Output (MIMO) transmission technology has been proposed as an advanced form of MIMO, in order to enhance channel capacity by virtually increasing the number of antennas through the collaboration of multiple user terminals (UTs). In collaboration among UTs, data sharing can be achieved efficiently by utilizing the high-frequency band, which is capable of high-capacity transmission, and the capacity improvement effect can be achieved by the collaborative MIMO transmission. As a detailed evaluation of uplink collaborative MIMO transmission, this section evaluates the throughput performance and verifies its effectiveness by considering the overhead required for cooperation such as data sharing.**

II-1.8.1. Introduction

Multiple-Input Multiple-Output (MIMO) technology, in which both the transmitter and receiver are equipped with multiple antennas and multiple signals are transmitted at the same time and frequency, has been continuously studied as an elemental technology for increasing capacity, and its practical application is also being promoted. As the number of antennas used increases, the upper limit on the amount of information that can be transmitted also increases. If the number of antennas on the user terminal (UT) side as well as on the base station (BS) can be increased, the communication capacity of uplink transmission can be improved. However, while it is relatively easy to increase the number of antennas on the BS side, it is difficult to install a large number of antennas on the UT side due to the size of the UT and spatial correlation. The challenge is to incorporate the various advantages of multi-element antennas in a limited physical space.

A method that has been devised to address this problem is to increase the number of antennas by linking multiple UTs, so that they can function as a single UT with a virtual large number of arrays [1][2]. This method is expected to improve transmission speed or communication quality without increasing the number of UT antennas. Terminal-collaborative MIMO has been mainly studied for improving downlink transmission performance [3][4]. In recent years, the effectiveness of UT selection [5], transmission path tracking, and error correction [6][7] in improving performance has been demonstrated in conjunction with experimental studies.

In this study, we focus on the uplink transmission of terminal-collaborative MIMO and formulate a detailed evaluation of the uplink transmission by considering the overhead

required for cooperation. Simulation based on the formulation clarifies its throughput performance more practically, and clarifies the area where it is advantageous.

II-1.8.2. System Model

The system model in the uplink of terminal-collaborative MIMO is shown in Figure II-1.8-1. BS shall be equipped with N antennas and shall communicate with a UT having only one antenna in the microwave band (Sub-6 band). Suppose there are Nu UTs under the cell of BS, M of them form a UT coordination group and perform uplink transmission to the BS. In this study, we focus on communication between collaborating UTs and MIMO communication between BS and cooperating UTs. Millimeter wave band (28GHz) is used for communication among UTs because of the relatively short distance and short overhead due to wideband transmission, and a line-of- sight (LoS) environment is assumed for the propagation path. Each UT has only one antenna, and a MIMO channel is constructed between M UTs linked to the BS.

The channel matrix $\mathbf{H} \in \mathbb{C}^{N \times M}$ can be expressed as

$$\mathbf{H} = \begin{bmatrix} h_{11} & h_{12} & \cdots & h_{1M} \\ h_{21} & h_{22} & \cdots & h_{2M} \\ \vdots & \vdots & \ddots & \vdots \\ h_{N1} & h_{N2} & \cdots & h_{NM} \end{bmatrix} \quad (1)$$

II-1.8.3. Procedure for Collaborative MIMO Uplink Transmission

The steps required to link UTs and transmit the uplink can be divided into four major categories. In this evaluation, the time required for each procedure is derived and the execution throughput is calculated. At this point, it is assumed that the source UT for coordination (the 1st UT in this simulation) and the UTs to be coordinated have already been determined. The variables used in this evaluation are summarized in Table II-1.8-1.

- CSI sharing.
- Data sharing.
- Weighted data stream sharing.
- Collaborative uplink transmission.

Table II-1.8-1. Parameter definitions.

Variable	Definition
N	Number of BS antennas
M	Number of UTs in collaboration
i, j	Indices of UTs
Nst	Number of MIMO streams
b_{csi}	CSI Data volume
b_{dat}	Information data volume
B_{uu}	UT-UT communication bandwidth
B_{ul}	Communication bandwidth between UT and BS
C_{ij}	Channel Capacity of the i-th and the j-th UTs
C_{ul}	UT-BS Uplink Channel Capacity
α	Guard interval efficiency
β	Guard band efficiency
γ	Modulation and coding efficiency

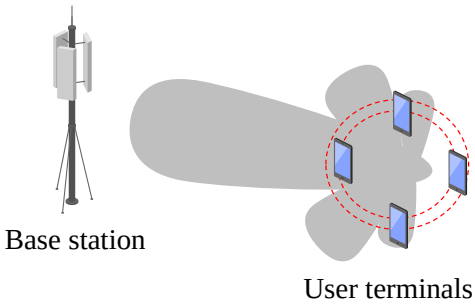

Figure II-1.8-1. Uplink transmission by virtual array.

II-1.8.3.1. CSI Sharing

First, the source UT collects channel state information (CSI) for uplink from collaborating UTs. Table II-1.8-2(a) shows an overview diagram of CSI and data sharing. The time required to collect CSI can be expressed as follows.

$$T_{\text{csi}} = \sum_{j=1,\, j\neq i}^{n_{\text{gr}}} \frac{b_{\text{csi}}}{B_{\text{uu}} C_{ij}} \tag{2}$$

In this case, the channel capacity C_{ij} [bit/s/Hz] between user the i-th and the-j UTs is calculated as follows.

$$C_{ij} = \log_2(1 + \text{SNR}_{\text{uu}}) \times \alpha \times \beta \times \gamma \tag{3}$$

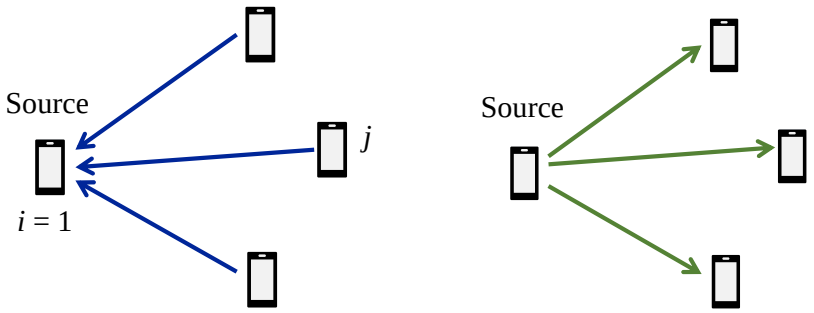

(a) CSI and data sharing (b) Feedback of weighted signal

Figure II-1.8-2. Signaling for collaborative transmission: UTs take turns transmitting and sharing their signals.

II-1.8.3.2. Data Sharing

Next, data to be sent from each UT is collected at the reference UT in turn. The duration required for this process is calculated as follows. Note that the number of streams is the same as the number of cooperating UTs.

$$T_{dat1} = \sum_{j=1,\, j\neq i}^{N_{st}-1} \frac{b_{dat}}{B_{uu} C_{ij}} \tag{4}$$

II-1.8.3.3. Weighted Signal Sharing

Then, the weighted data is shared to each UT in turn, starting from the UT that is the reference. Table II-1.8-2(b) shows a schematic diagram of the weighted signal sharing process. The period required for this process is calculated as follows. The UT coordination is completed by this procedure.

$$T_{\mathrm{dat2}} = \sum_{j=1,\, j\neq i}^{N_{\mathrm{st}}-1} \frac{b_{\mathrm{dat}}}{B_{\mathrm{uu}} C_{ij}} \tag{5}$$

II-1.8.3.4. Uplink Transmission

Finally, data is transmitted from the coordinated UT to BS. The duration required for this process is calculated as follows.

$$T_{\mathrm{ul}} = \frac{b_{\mathrm{dat}}}{B_{\mathrm{ul}} C_{\mathrm{ul}}} \tag{6}$$

The uplink transmission channel capacity C_{ul} [bit/s/Hz] is calculated as follows.

$$C_{\mathrm{ul}} = \log_2(1 + \mathrm{SNR}_{\mathrm{ul}}) \times \alpha \times \beta \tag{7}$$

II-1.8.3.5. Effective Throughput

The effective throughput TP is calculated as follows. The effective throughput indicates the delivered information bits per unit time.

$$\mathrm{TP} = \frac{N_{\mathrm{st}} b_{\mathrm{dat}}}{T_{csi} + T_{\mathrm{dat1}} + T_{\mathrm{dat2}} + T_{\mathrm{ul}}} \tag{8}$$

From the equation (8), TP can be improved by shortening the time until uplink transmission. To reduce coordinating overhead, it is effective to increase the channel capacity between cooperating UTs, as shown in Equations (2)–(5).

II-1.8.4. Performance Evaluation

II-1.8.4.1. Simulation Parameters

As parameters for this simulation, Table II-1.8-2 shows the settings for UT–UT communication, and Table II-1.8-3 shows the settings for UT–BS communication. For the carrier frequency, we assume that the Sub6 band is used for communication between UTs and BSs, and that millimeter wave is used for coordination between UTs, since we assume a situation where UTs are in close proximity to each other. 20 UTs with single antenna are randomly placed within a radius of 5 m, and time variation in UT placement is not considered. The MIMO transmission method assumes that CSI can be shared between the transmitting and receiving sides, and E-SDM transmission is used. The number of UTs within a specified range is varied to evaluate the impact of the number of coordinated UTs on communication capacity. Figure II-1.8-3 shows an example of the location relationship using the case where five UTs are collaborating.

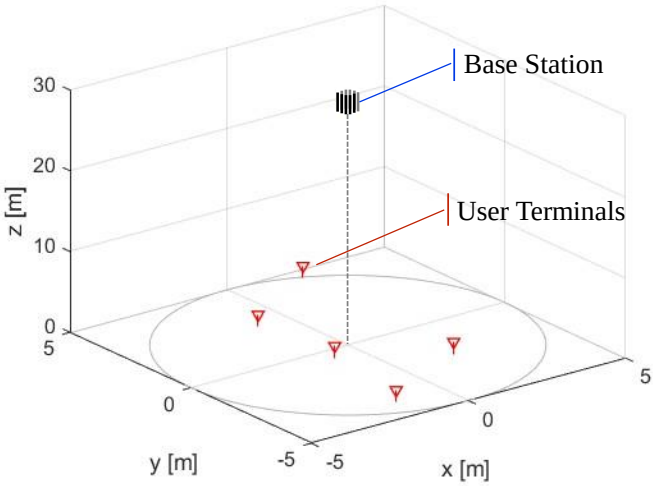

Figure II-1.8-4. Simulation environment.

Table II-1.8-2. Parameters for UT–UT communication.

Parameter	Value
Carrier Frequency	28 GHz
Transmission bandwidth	400 MHz
Transmission power	24 dBm
Antenna gain	0 dBi
Noise figure	9 dB
CSI data volume	12 bits
Information data volume	1.2×10^5 bits
Guard interval efficiency	0.9
Guard band efficiency	0.8
Modulation Coding Efficiency	0.3
Channel model	Line-of-Sight

Table II-1.8-3. Parameters for UT–BT communication.

Parameter	Value
Carrier frequency	3.65 GHz
Transmission bandwidth	20 MHz
Antenna gain	0 dBi
Guard interval efficiency	0.9
Guard band efficiency	0.8
MIMO transmission method	E-SDM
Channel model	i.i.d Rayleigh

II-1.8.4.2. Simulation Results

Figure II-1.8-4 shows the effective throughput performance when the SNR between the UT and the BS is varied from 0 to 30 dB in 10 dB increments and the number of coordinated UTs M is varied from 1 to 20. The number of transmitted streams is the same as the number of UTs. The figure shows that the throughput is higher when the number of coordinated UTs is two or more, i.e., when they are coordinated, in all SNR situations. The effect of coordination is particularly strong at low SNR. The throughput increases as the number of coordinated UTs increases, but when the number of coordinated UTs is approximately 10 or more, the effect of the overhead of inter-UT communication in coordination becomes significant. At high SNRs such as 30 dB, the overhead of UT–UT communication is relatively dominant compared to uplink transmission, limiting the increase in throughput, suggesting room for improvement.

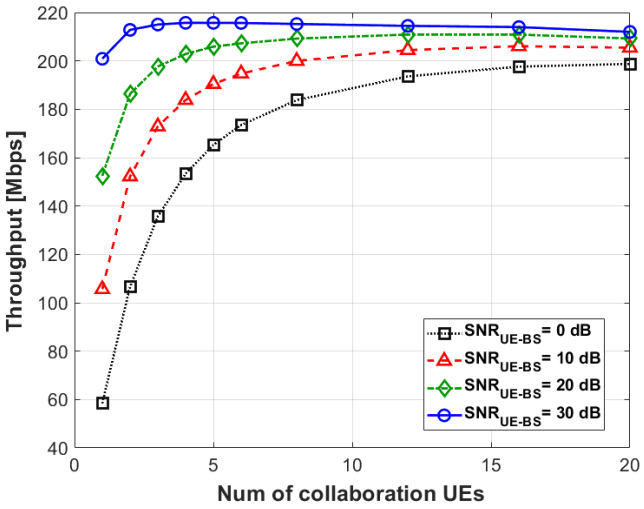

Figure II-1.8-5. Median throughput of collaborative transmission.

To examine the effect of terminal collaboration in detail, the number of transmit streams is set to 1, and the throughput is calculated when the power used by the UT is varied from full power (= 1), 1/4, and 1/10. The SNR between UT and BS is assumed to be 0 dB or 10 dB. The results are shown in Figure II-1.8-5. When the SNR is low (0 dB), the throughput improves with coordination, even if the power consumption of the UT is reduced. This result suggests that both energy and communication capacity can be achieved. However, when the SNR is 10 dB, the coordination effect is significantly affected by the overhead caused by the coordination, indicating that there is room for improvement.

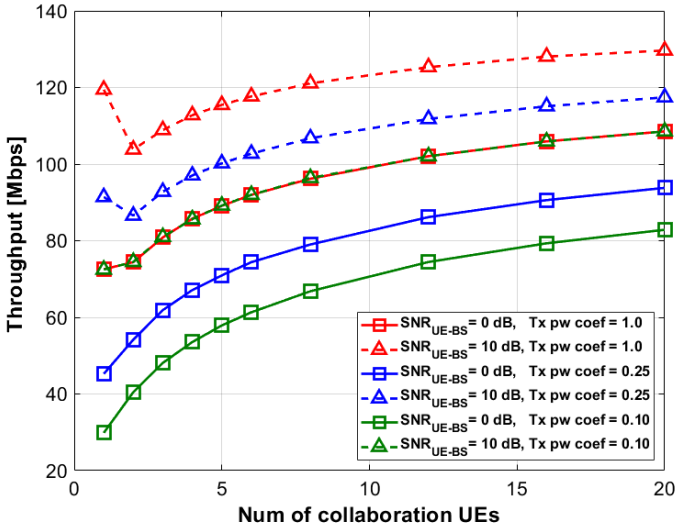

Figure II-1.8-6. Median throughput of collaborative transmission (single stream).

II-1.8.5. Conclusion

As an advanced form of MIMO transmission technology, which uses multiple antennas to transmit and receive multiple different signals in wireless communications, terminal-collaborative MIMO transmission technology has been proposed to increase the number of antennas and improve the channel capacity by coordinating multiple wireless UTs. In coordination between UTs, data sharing can be achieved efficiently by utilizing the high-frequency band, which is capable of large-capacity transmission, and the capacity improvement of coordinated MIMO transmission can be obtained. In this study, as a detailed evaluation, we evaluated the effective throughput performance of uplink terminal-collaborative MIMO transmission by formulation and simulation considering the signaling overhead required for coordination, and confirmed the effectiveness of this method. Future work includes exploring further effectiveness of the collaboration by selecting the UTs, taking into account the inter-UT distance and the strength of uplink SNR.

REFERENCE

[1] M. Dohler, J. Dominguez, and H. Aghvami, "Link capacity analysis for virtual antenna arrays," in *Proceedings IEEE 56th Vehicular Technology Conference*, vol. 1, 2002, pp. 440–443 vol.1.

[2] M. Kasai and H. Murata, "Performance comparison of adaptive terminal selection schemes for terminal-collaborated MIMO reception using actual received signals," in *2020 IEEE 91st Vehicular Technology Conference (VTC2020-Spring)*, 2020, pp. 1–5.

[3] R. Dabora and S. D. Servetto, "Broadcast channels with cooperating decoders,"

[4] *IEEE Transactions on Information Theory*, vol. 52, no. 12, pp. 5438–5454, 2006.

[5] H. Kwon and J. M. Cioffi, "Multi-user miso broadcast channel with user-cooperating decoder," in *2008 IEEE 68th Vehicular Technology Conference*, 2008, pp. 1–5.

[6] H. Murata, "Terminal selection schemes in terminal-collaborated MIMO reception based on subband channel matrices," *IEEE Communications Letters*, vol. 26, no. 1,

[7] pp. 202–206, 2022.

[8] H. Taromaru and H. Murata, "Performance comparison of error-control schemes in collaborative multiple-input multiple-output systems," in *2022 IEEE 96th Vehicular Technology Conference (VTC2022-Fall)*, 2022, pp. 1–5.

[9] H. Taromaru, H. Murata, T. Nakahira, D. Murayama, and T. Moriyama, "Error control on mobile station sides in collaborative multiple-input multiple-output systems," *IEEE Access*, vol. 10, pp. 26 493–26 500, 2022.

II-2. Virtualized Terminal Technology using Terahertz-Band for Ultra High Capacity towards Beyond 5G and 6G

Kazuki Takezawa, Satoshi Ito, Yoshio Kunisawa, Takeo Ooseki, Tatsuya Nagao, and Takahiro Hayashi
KDDI Research, Inc.

Abstract— **In the near future, advancements in Cyber-Physical Systems (CPS) that integrate physical space and cyberspace are expected to lead to a prosperous era for society. To achieve this, it is necessary to support ultra-high-capacity data transmission through new wireless systems such as Beyond 5G and 6G. The terahertz band offers great potential for such high-capacity communication; however, challenges such as significant propagation loss and attenuation also exist. This section presents the concept of a virtualized terminal that combines terahertz and millimeter wave technologies to enable high-capacity data transmission in Beyond 5G/6G networks. We detail the configuration of this terminal, particularly the utilization of the 300 GHz band. Additionally, we conducted simulations to evaluate the transmission performance while walking, revealing that maintaining LOS between the UE and the Relay Device (RD) is crucial for optimal performance. Experiments using prototype hardware demonstrated the feasibility of polarization multiplexing in the terahertz and millimeter wave bands. In these experiments, a transmission speed of approximately 19.07 Gbps was achieved over short distances, although performance fluctuated due to hardware constraints.**

II-2.1. Introduction

With the advent of 5G services, research and development towards the next-generation technologies Beyond 5G and 6G have accelerated. The 2030s, projected as the era for the realization of Beyond 5G, envision a society where “everyone can thrive,” “sustainable growth is achieved,” and “activities can be conducted with a sense of security.” This societal transformation is anticipated to be realized within Society 5.0, where the integration of physical and cyber spaces, known as Cyber-Physical Systems (CPS), will have advanced significantly [1]. To establish CPS, it is essential to transfer data replicating the physical space into cyber space and reproduce the information generated and processed in cyberspace back into the physical space using technologies such as high-definition 3D images and holograms. The wireless systems of Beyond 5G, which are vital for these realizations, must provide high communication performance adaptable to the communication environment and individual demands of users in any location. Moreover, the capability to transfer vast amounts of data, including both downlink and uplink, significantly surpassing current levels, is crucial.

To realize ultra-high-capacity communications anticipated in Beyond 5G and 6G, the utilization of the terahertz band exceeding 100 GHz is being explored. The International Telecommunication Union Radiocommunication Sector (ITU-R) has allocated the terahertz band from 252 GHz to 296 GHz for land mobile services [2]. This band offers the potential for ultra-wideband transmission with a bandwidth of 44 GHz, making it promising for ultra-high-capacity communications. However, the terahertz band is characterized by significant propagation losses and high attenuation due to obstructions, which may limit coverage when used with conventional mobile communication system access links. To address this challenge and achieve ultra-high-capacity transmission and coverage, the authors proposed a virtualized terminal combining terahertz and millimeter waves for relay transmission [3].

This section presents the evaluation results of the virtualized terminal designed to realize high-capacity communications in the Beyond 5G/6G era. Section II-2-2 introduces the overview and configuration of the virtualized terminal. Section II-2-3 reports the results of simulations evaluating the physical transmission rate during walking, a scenario where the virtualized terminal is expected to be utilized. Section II-2-4 presents the results of empirical experiments conducted with the prototype hardware of the virtualized terminal. Finally, Section II-2-5 provides a summary and discusses future prospects.

II-2.2. Virtualized Terminal using THz-band

The concept of the virtualized terminal is shown in Figs. II-2-1. The virtualized terminal consists of a user equipment (UE), equivalent to a smartphone, and relay devices (RDs), corresponding to wearable devices. In the virtualized terminal, the antenna functions of the UE are transferred to wearable devices and other nearby wireless devices, effectively creating a terminal with a large number of virtual antennas. This configuration aims to achieve transmission capacity of up to 100 Gbps by increasing the number of antennas without physical constraints, thereby enhancing the spatial multiplexing capability of MIMO systems. Additionally, to ensure high-capacity wireless connections between the RDs with transferred antenna functions and the UE, the terahertz band, which supports ultra-wideband transmission, is utilized. Specifically, this study examines the use of the 300 GHz band (252 GHz - 296 GHz) for these connections.

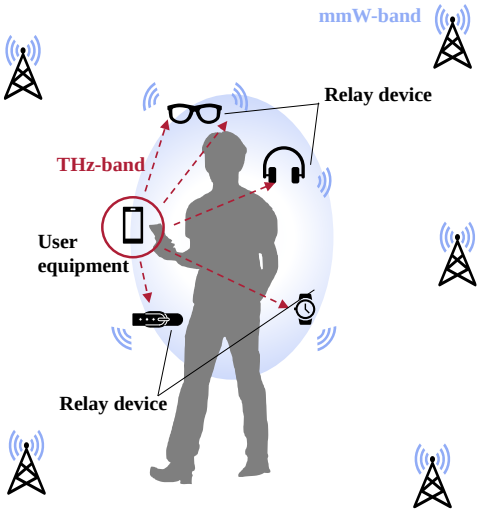

Fig. II-2-1. The concept of the virtualized terminal, which uses wireless devices wearing a human body as relay devices.

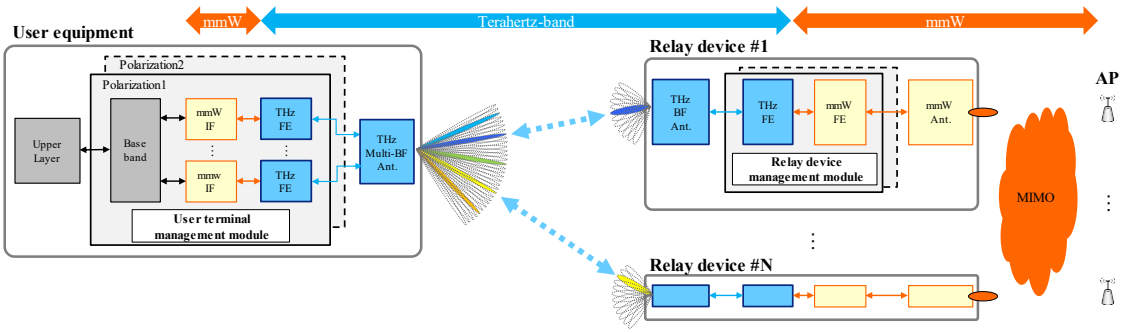

Fig. II-2-2. The structure of the virtualized terminal.

The configuration of the virtualized terminal is depicted in Fig. II-2-2. The flow of uplink transmission in the virtualized terminal configuration is explained as follows. Data sequences transmitted from the UE are modulated into millimeter-wave signals by the baseband unit and then frequency-converted to the terahertz band by the terahertz RF unit, which inputs them into the terahertz multi-beam antenna. Using multi-beam polarization division multiplexing transmission from the antenna makes simultaneous connections with multiple RDs possible. To mitigate interference among the multi-beams, a component carrier with a bandwidth of 4.8 GHz, similar to the millimeter-wave band, is allocated to each RD. The terahertz signals received by the RDs are frequency-converted to millimeter-wave signals and then radiated towards the access points (APs). This virtualized terminal configuration increases the number of RDs, thereby enhancing

the MIMO multiplexing capability with the AP and expanding the communication capacity.

II-2.3. Simulation Evaluation

The virtualized terminal assumes the utilization of the terahertz band in the vicinity of a moving human body. Due to significant attenuation caused by obstructions like the human body, the performance of the virtualized terminal can vary greatly depending on actual operational scenarios and the placement of RDs. Therefore, simulations were conducted using the propagation characteristics of radio waves near the human body, modeled based on empirical measurements [4] [5].

The simulation environment is shown in Fig. II-2-3. It is assumed that the evaluation target APs are uniformly distributed, maintaining a distance of 200 meters. Each RD that constitutes the virtualized terminal is assumed to communicate with the five nearest APs. In this AP configuration environment, the user holds the UE in their right hand, and the RDs are attached to the right and left ears of headphones, the forehead part of a hat, the left wrist of a watch, and the abdomen of a belt. The simulation mimics a walking action for approximately 2.5 seconds. In this simulation, it is assumed that the non-linear distortion compensation technology and terahertz beam control technology, which are part of the virtualized terminal configuration, can be ideally applied. Each RD transmits QPSK signals via polarization multiplexing, achieving a maximum physical transmission rate of 96 Gbps.

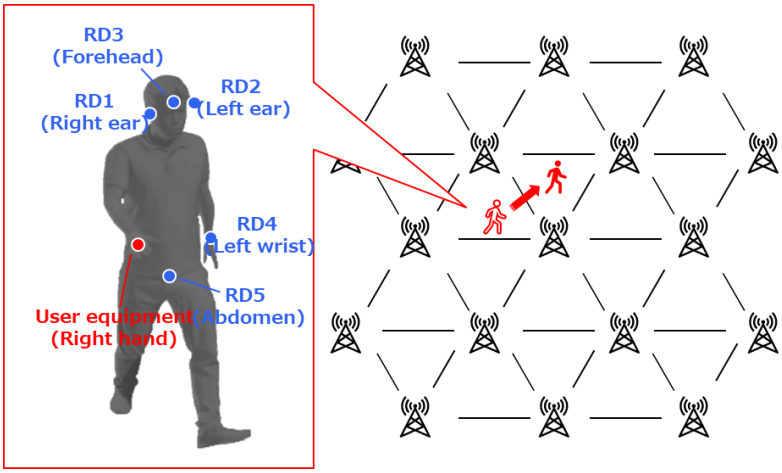

Fig. II-2-3. Simulation environment to evaluate the performance of the virtualized terminal.

Fig. II-2-4 shows the time variation of the physical transmission rate obtained through the simulation. At around 0.3 seconds, 1.5 seconds, and 2.5 seconds, the maximum rate of 96 Gbps is achieved, indicating that the maximum transmission rate can be obtained under specific conditions. Conversely, the physical transmission rate deteriorates around 0.5 to 1.0 seconds and 1.8 to 2.4 seconds. This deterioration is attributed to the degradation of communication quality in the terahertz band wireless part during these periods.

Fig. II-2-5 shows the time variation of the propagation loss between the UE and each RD. The vertical axis represents the value obtained by subtracting the antenna gain of the UE and RD from the propagation loss in the terahertz wireless section, indicating the loss in the terahertz wireless section. Significant increases in loss at the times when the physical transmission rate deteriorates in Fig. II-2-4 suggest that the right hand holding the UE is positioned behind the body, obstructing the line of sight (LOS) with each RD.

These results indicate that the quality of the terahertz band wireless part highly influences the performance of the virtualized terminal during the assumed walking motion. In particular, communication quality significantly deteriorates when the LOS between the UE and RDs is lost. Therefore, maintaining the LOS between the RDs and the UE is crucial to maximizing the performance of the virtualized terminal in real-world scenarios. Although this simulation evaluated a configuration with five RDs, methods that involve switching to appropriate RDs while maintaining a more significant number of RDs may be necessary.

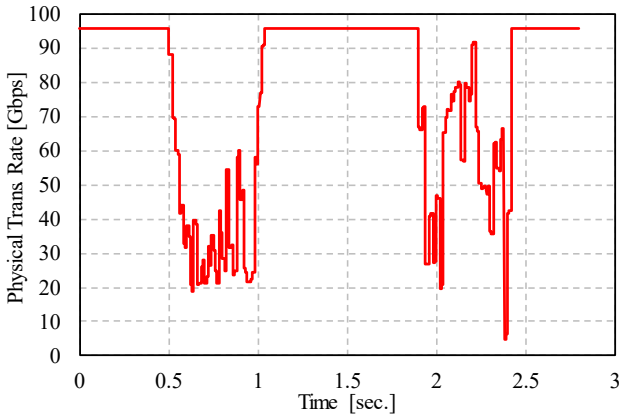

Fig. II-2-4. Time variation of the physical transmission rate of the virtualized terminal.

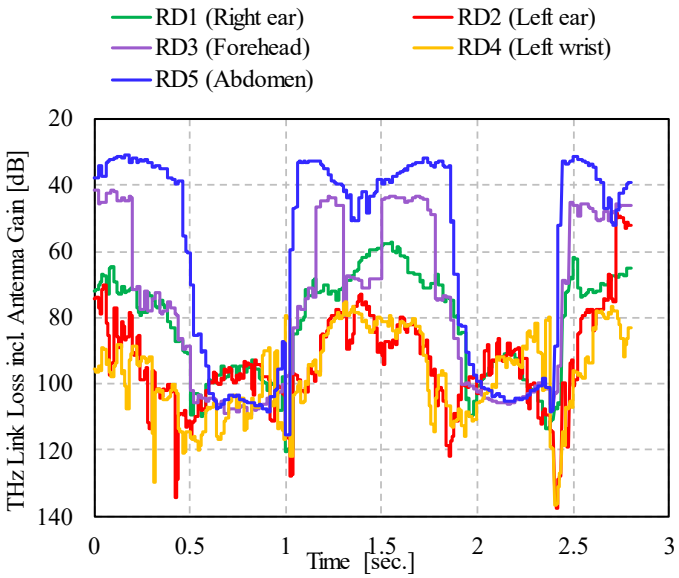

Fig. II-2-5. Time variation of transmission loss in the terahertz links with each relay device.

II-2.4. Experimental Results

Fig. II-2-6 shows an overview photograph of the demonstration experiment and an enlarged photo of the terahertz section. In this demonstration experiment, an OFDM signal (1st modulation: QPSK) was generated using an arbitrary waveform generator and input into the UE. The center frequency was 37.5 GHz with a bandwidth of 4.8 GHz. The UE converted the frequency to terahertz band signals with a center frequency of 265.2 GHz and a bandwidth of 4.8 GHz, which were then input into a spherical lens antenna [6]. At the RD, the terahertz wave was received by a plano-convex lens antenna [6], frequency-converted back to 37.5 GHz, and transmitted to the AP via a dual-polarization millimeter-wave antenna. The physical transmission rate was calculated and evaluated by observing the signal on an oscilloscope and measuring the Bit Error Rate (BER). In this experimental setup, vertical and horizontal polarization antennas were connected to the UE and RD to support orthogonal polarization transmission.

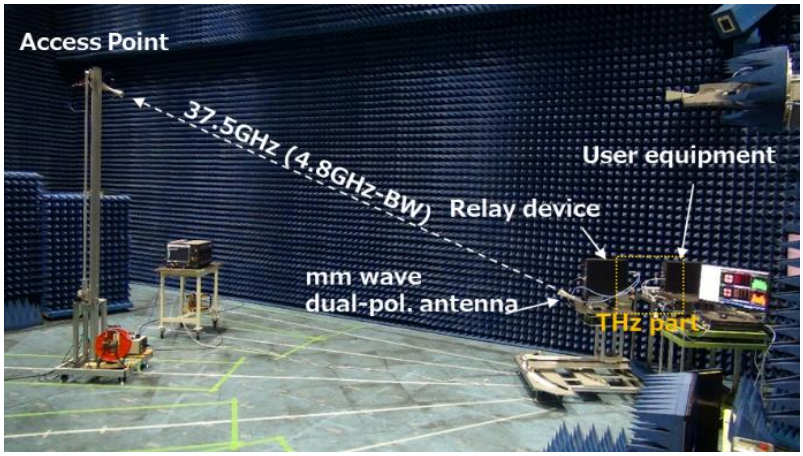

(a) Photograph of whole part of the measurement setup.

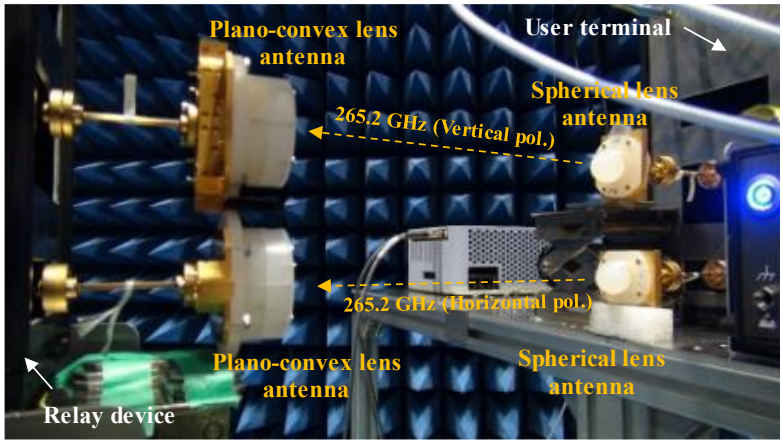

(b) Photograph zoomed up terahertz-band part.

Fig. II-2-6. Photographs at the time of the measurement.

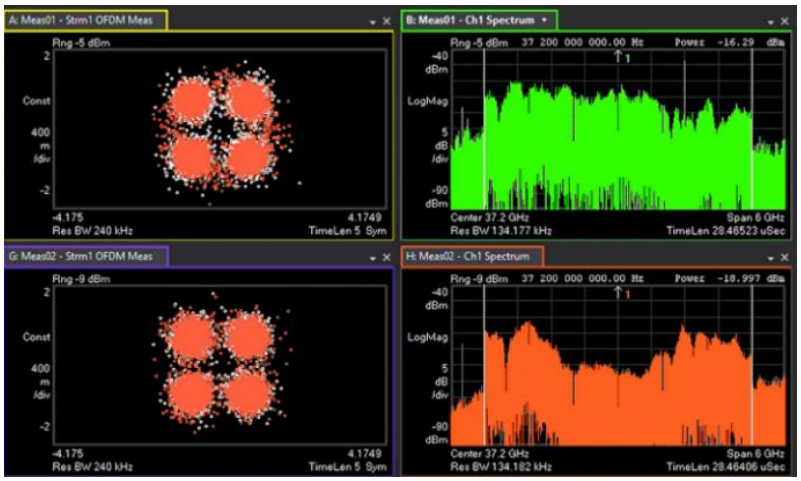

Fig. II-2-7. Transmission characteristics of the virtualized terminal in the demonstration experiment (upper: vertical polarization system, lower: horizontal polarization system).

The results of this demonstration experiment are described below. Fig. II-2-7 shows the constellation and frequency characteristics of the demodulated signal at the oscilloscope. The upper row represents the vertical polarization system, while the lower row represents the horizontal polarization system. The transmission distance for the millimeter-wave was set to 5 meters, and the transmission distances for the terahertz band's vertical and horizontal polarization systems were set to 20 cm each. As shown in Fig. II-2-7, the QPSK modulated signal was demodulated mainly correctly. The BER of the demodulated signal was 1.11% for the vertical polarization system and 0.25% for the horizontal polarization system, resulting in a total transmission rate of 19.07 Gbps for both polarizations. This demonstrates that the virtualized terminal can achieve transmission in principle even in environments with polarization interference in both the terahertz and millimeter-wave bands. However, when the transmission distance in the terahertz band was extended to 50 cm, the vertical polarization system could not be demodulated, and only the horizontal polarization system achieved a transmission rate of 9.34 Gbps. The terahertz band RF part of the prototype wireless devices showed significant variations between devices, as indicated by the different frequency characteristics shown on the right side of Fig. II-2-7. This likely resulted in only the horizontal polarization system being capable of communication. Future work will require performance evaluations with multiple RDs and improvements in hardware performance to achieve longer-distance transmission in both the millimeter-wave and terahertz bands.

II-2.5. Conclusion

This section introduced the virtualized terminal proposed by the authors to realize ultra-high-capacity communications anticipated in Beyond 5G and 6G. Simulations demonstrated that it is possible to achieve communication capacity of up to 100 Gbps during basic operations such as walking. However, since the performance characteristics significantly vary depending on the LOS conditions, it is necessary to explore methods such as utilizing more RDs. In the hardware-based demonstration experiment, polarization multiplexing transmission was conducted in both the terahertz and millimeter-wave bands, achieving the target rate of approximately 19.2 Gbps with a single RD. Future work will focus on miniaturization and performance enhancement by integrating terahertz band antennas and terahertz RF circuits in RDs. Additionally, demonstration experiments will be conducted to show that physical transmission speeds can be expanded by using multiple RDs.

Acknowledgement

These research results were obtained from commissioned research (JPJ012368C00401) by the National Institute of Information and Communications Technology (NICT), Japan.

We would like to sincerely thank Prof. Nakabayashi of Chiba Institute of Technology for providing us the propagation channel and Prof. Sakakibara and Assistant Prof. Sugimoto of Nagoya Institute of Technology for lending us the teraherz-band antennas.

REFERENCE

[1] Ministry of Internal Affairs and Communications Japan, “aBeyond 5G Promotion Strategy—Roadmap towards 6G—,”

https://www.soumu.go.jp/main_sosiki/joho_tsusin/eng/pressrelease/2020/6/30_7.html, June, 2020.

[2] ITU-R, “World Radiocommunication Conference 2019 Final Acts.”, 2019.

[3] KDDI corporation, KDDI Research, Inc., “Beyond 5G/6G White Paper ver.2.0.1,” Oct. 2021, https://www.kddi-research.jp/english/tech/whitepaper_b5g_6g/

[4] K. Takezawa, S. Ito and T. Hayashi, "Estimation Method for Human Blockage Loss in the 300 GHz Band," 2023 IEEE 98th Vehicular Technology Conference (VTC2023-Fall), Hong Kong, Hong Kong, 2023, pp. 1-5, doi: 10.1109/VTC2023-Fall60731.2023.10333370.

[5] K. Imaseki and H. Nakabayashi, “Basic Study of Time-Spatial Propagation Path near Human Body in 300 GHz Band Using Map-Based Hybrid Channel Model,” IEICE technical report, vol. AP2023-160, Jan. 2024.

[6] Y. Sugimoto, T. Tsuchida, T. Sugiyama, S. Kishi, A. Iwamoto, K. Nishimura, T. Narita, M. Sakamoto, K. Sakakibara, N. Kikuma, S. Ito, Y. Kunisawa and T. Hayashi, “Sub-THz Multi-Beam Antennas for Virtualized Terminal Technology”, 2024 Joint European Conference on Networks and Communications & 6G Summit (EuCNC/6G Summit), pp. 711-716, 2024.

II-3. Performance of Collaborative MIMO Reception: Initial Results of 25.9GHz Collaboration

Hidekazu Murata
Yamaguchi University,
Shoko Shinohara, Toshiro Nakahira, Takeru Fukushima, Daisuke Murayama,
and Yusuke Asai
NTT Access Network Service System Laboratories

Abstract— **This section presents initial experimental results of a collaborative MIMO reception system utilizing high-frequency bands for inter-terminal communication. To overcome antenna correlation issues in compact mobile devices, multiple terminals receive four-stream MIMO signals transmitted from a base station and share the digitized signals with a central terminal over a 25.9 GHz band. Experiments conducted on a university campus demonstrated successful decoding with reasonable bit error rates, even under varying numbers of collaboration terminals. The results indicate the feasibility of enhancing spectral efficiency through terminal collaboration using high-frequency links in MIMO systems.**

II-3.1. Introduction

Multiple-input multiple-output (MIMO) transmission improves spectral efficiency by simultaneously transmitting multiple independent signals using multiple antennas at both the transmitter and receiver over the same frequency and time. As is well known, the channel capacity of MIMO systems is approximately proportional to the minimum of the number of transmit and receive antennas. However, in compact mobile devices such as smartphones, installing a large number of antennas is challenging due to limited space, resulting in high correlation between signals and degraded transmission performance. To address this issue, collaborative MIMO reception among neighboring terminals has been studied [1,2], aiming to enhance transmission performance by leveraging collaboration among nearby devices.

In this collaborative MIMO reception scheme, multiple wireless terminals receive MIMO signals transmitted from a base station (BS), and the received signals are shared among the collaborating terminals. This enables the group of terminals to function as a virtual device with multiple antennas. Since the distance between collaborating terminals is generally larger than the carrier wavelength, the signal correlation is low, and improved MIMO performance can be expected.

While increasing the number of collaborating terminals enhances transmission performance, it also raises the issue of increased wireless traffic required for inter-

terminal communication. This study proposes using high-frequency bands for this collaborative communication. By utilizing high-frequency bands for short-range inter-terminal communication, the proposed collaborative MIMO system aims to improve the spectral efficiency of valuable bands such as the UHF band.

In this section, we present initial experimental results of a system in which four-stream MIMO signals are transmitted over a university campus, and six terminals collaborate using high-frequency bands to receive the signals.

II-3.2. System Model

Fig. II-3-1 shows the experimental system configuration. The BS transmits four independent MIMO signal streams via spatial multiplexing. The BS consists of a software-defined radio (SDR) device with four ports, controlled by a single computer. On the receiver side, six mobile stations (MSs), each equipped with a single antenna, receive the MIMO signals and share the digitized waveforms. In this experiment, all received signals were forwarded to a single MS over high-frequency bands. Each MS comprises an SDR, a control computer, and frequency converters. In the figure, "UP" denotes an upconverter and "DOWN" denotes a downconverter. Decoding is performed via frequency domain iterative equalization, and the results are sent to a recording computer (Rec PC). These processes are executed in real-time on a 50 ms frame basis [3].

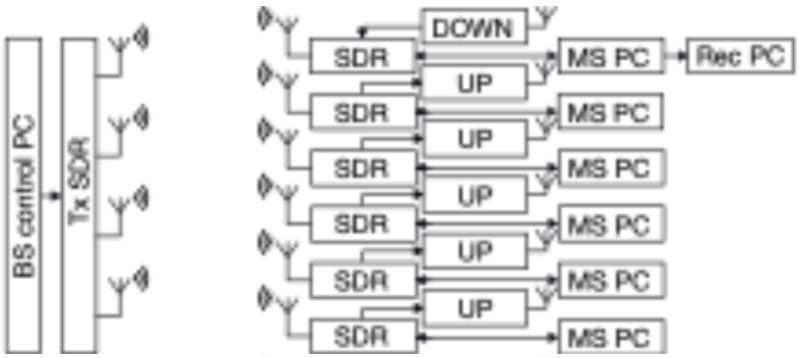

Fig. II-3-1 System model of terminal-collaborated MIMO reception system.

II-3.3. Measurement Campaign

As shown in Fig. II-3-2, the BS antennas were installed in a uniform linear array (ULA) configuration on the rooftop of a building (approximately 31 meters above ground) at the Tokiwa campus of Yamaguchi University, with an inter-element spacing of 2.8

meters. The transmitted signal frequency from the BS was 427.2 MHz, and the symbol rate was 312.5 ksps. As shown in Fig. II-3-3, the six receiver MSs were located approximately 143 meters away in a courtyard. The received and digitized signals were forwarded to terminal MS1 over the 25.9 GHz band. Five of the MSs were evenly spaced along a circular path with a 4-meter radius, moving around the circle every 42 seconds. MS1 was placed at the center, and performed decoding using both the received signals from other MSs and its own received signal. Frequency and timing synchronization were

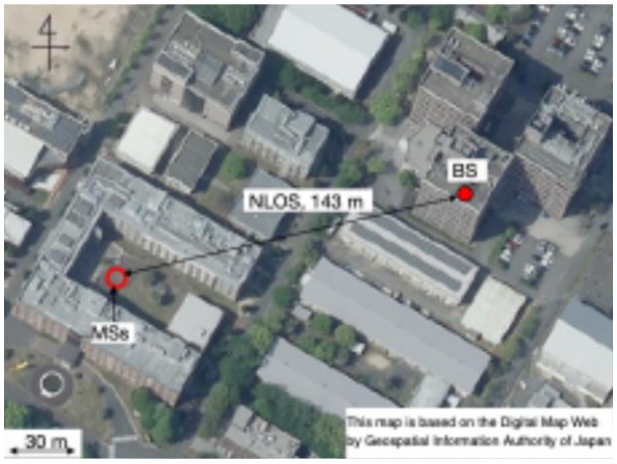

Fig. II-3-2 Measurement campaign field and layout.

achieved using GPS-based 10 MHz and 1PPS (Pulse Per Second) signals. The average received signal power from the BS was −75.4 dBm.

Fig. II-3-3 MSs at receiver side.

Simple horn antennas and a wide-beamwidth directional antenna (shown in Fig. II-3-4) were used for high-frequency band communication. Terminals arranged along the circular path used horn antennas directed toward the central MS1. The MS1 was

equipped with an upward-facing wide-beamwidth directional antenna. The antenna radiation patterns are shown in Fig. II-3-5.

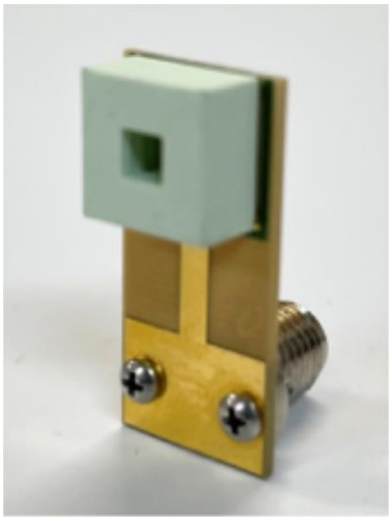

Fig. II-3-4 Wide-beamwidth directional antenna (Niterra Co., Ltd.).

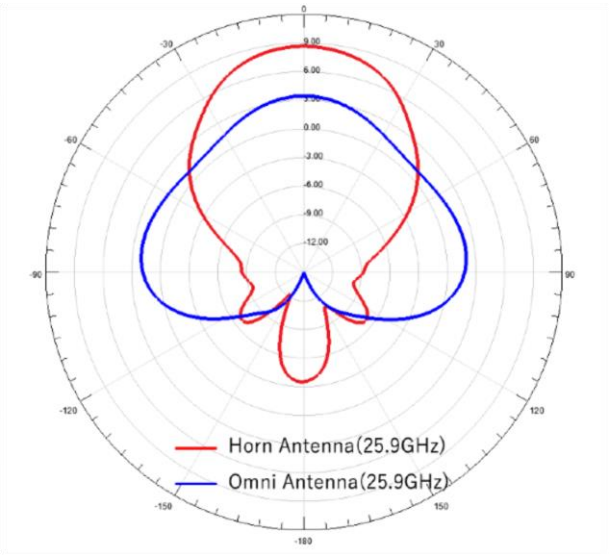

Fig. II-3-5 H-plane radiation pattern of wide-beamwidth directional antenna.

II-3.4. Experimental Results

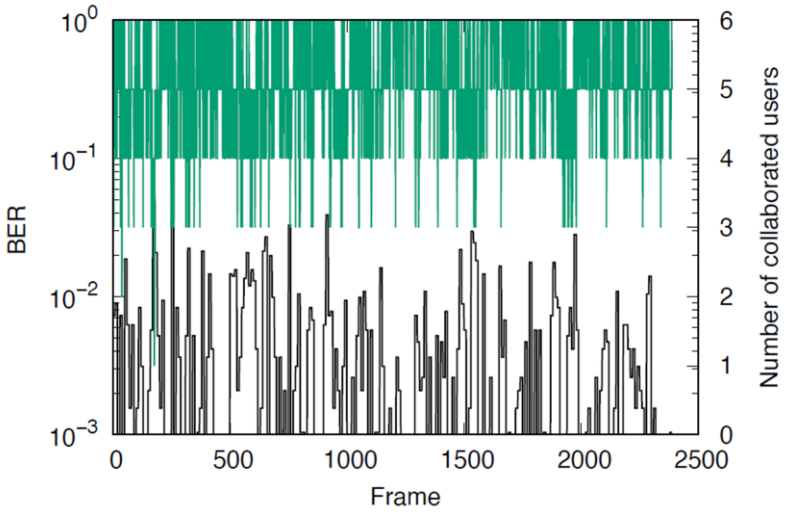

Fig. II-3-6 BER averaged over 10 packets and number of collaborated MSs.

Fig. II-3-6 presents the experimental results. The black curve (left axis) shows the bit error rate (BER) averaged over 10 packets, while the green curve (right axis) indicates the number of received signal waveforms used for decoding. The horizontal axis shows the elapsed frame count. The results indicate that, in the current implementation, the number of collaborating MSs varied between three and six (i.e., six to three received signals), likely due to imperfect line-of-sight during the experiment and multipath interference. The BER performance remained around 10^{-2} or lower, suggesting a certain level of successful four-stream MIMO reception.

II-3.5. Conclusion

We have reported the initial experimental results of a collaborative MIMO system. Future work will focus on improving the inter-terminal communication component.

Acknowledgements

This work was supported in part by JSPS KAKENHI Grant Number JP23H00474.

REFERENCE

[1] F. Du, H. Murata, M. Kasai, T. Nakahira, K. Ishihara, M. Sasaki and T. Moriyama "Distributed detection of MIMO spatial multiplexed signals in terminal collaborated reception," IEICE Trans. Commun., vol. E104.B, no. 7, pp. 884-892, July 2020.

[2] H. Taromaru, H. Murata, T. Nakahira, D. Murayama, T. Moriyama, “Error control on mobile station sides in collaborative multiple-input multiple-output systems,” IEEE Access, Vol. 10, pp. 26493-26500, Mar. 2022.
[3] H. Sugai, H. Murata, X. Du, S. Shinohara, D. Murayama, T. Nakahira, T. Fukushima, Y. Asai, “Performance evaluation of collaborative MIMO reception system with multiple detection terminals using actual received signal,” IEICE Technical Report, RCS2024-280, pp. 108-113, Mar. 2025.

Abbreviation List

Abbreviation	Explanation
5G	Fifth-generation Mobile Communication System, Fifth-generation
AF	Amply-and-Forward
AWGN	Additive White Gaussian Noise
B2U	BS-to-UE
BER	Bit Error Rate
BF	Beamforming
BS	Base Station
CDF	Cumulative Distribution Function
CE	Channel Estimation
CIM	Color Images Method
C-MIMO	Chaos-Multiple-Input Multiple-Output
CPE	Common Phase Error
CPS	Cyber-Physical Systems
CRC	Cyclic Redundancy Check
CTFI	Complex Time Frequency Interferometry
CSI	Channel State Information
D2D	Device-to-device
DCF	Distributed Coordination Function
DF	Decode-and-Forward
DFC	Distributed Coordination Function
DFT	Discrete Fourier Transform
EHF	Extra High Frequency
FEC	Forward Error Correction
FER	Frame Error Rate
FFT	Fast Fourier Transform
FSS	Frequency Symbol Spreading
GI	Guard Interval
ICI	Inter-carrier Interference
IFFT	Inverse Fast Fourier Transform

Abbreviation	Explanation
ITU-R	International Telecommunication Union Radiocommunication Sector
LOS	Line-of-Sight
MIMO	Multi-Input Multi-Output
MLSE	Maximum Likelihood Sequence Estimation
MMSE	Minimum Mean Squared Error
MS	Mobile Station
NLOS	Non-Line-of-Site
OFDM	Orthogonal Frequency Division Multiplexing
PC	Power Control
PER	Packet Error Rate
PN	Phase Noise
PPS	Pulse Per Second
P/S	Parallel-to-Serial
QPSK	Quadrature-Phase Shift Keying
RD	Relay Device
Rec PC	Recording Computer
RMS	Relay Mobile Station
RS	Relay Stations
RTM	Ray Tracing Method
SDR	Software Defined Radio
SINR	Signal-to-Interference-plus-Noise Ratio
SNR	Signal-to-Noise Ratio, Signal-to-Noise Power Ratio
S/P	Serial-to-Parallel
TCCS	Terminal Cooperative Communication System
TMS	Target Mobile Station
UE	User Equipment
ULA	Uniform Linear Array
UT	User Terminal
VAA	Virtual Antenna Arrays
WHT	Walsh Hadamard Transform
WI	Wireless InSite

Abbreviation	Explanation
WLAN	Wireless Local Area Network
ZF	Zero-Forcing